

Teknillinen korkeakoulu. Konetekniikan osasto. LVI-tekniikan laboratorio. B
Helsinki University of Technology. Department of Mechanical Engineering.
Laboratory of Heating, Ventilating and Air Conditioning. B
Espoo 2003

MODELLING BRISTLE BEHAVIOUR IN
ROTATING BRUSH DUCT CLEANING

REPORT B75

Rauno Holopainen Eero-Matti Salonen

Helsinki University of Technology
Department of Mechanical Engineering
Laboratory of Heating, Ventilating and Air Conditioning

Distribution:

Helsinki University of Technology

Laboratory of Heating, Ventilating and Air Conditioning

P.O. Box 4100

FIN-02015 HUT

Tel. +358 9 451 3601

Fax. +358 9 451 3611

ISBN 951-22-6581-8

ISSN 1455-2043

Otamedia

Espoo 2003

ABSTRACT

The bristle of a rotating cleaning brush for air ducts was modelled using large deformation elastic theory. The point collocation method with a trial solution consisting of undetermined parameters was employed to discretize the resulting non-linear problem. The main interest was in determining the value of the bristle tip contact normal force N , the bristle tip contact angle β and the torque T needed to rotate a brush. The results obtained using the simple model were compared with the results obtained from a laboratory test.

The simulated and experimental results show that the magnitude of the normal force and the contact angle increase as a function of the rotation speed n . Additionally, the torque increases with the growth of the normal force. The results show further that air drag increases the torque and somewhat decreases the contact force between a bristle tip and the duct surface. However, with the normal properties of a brush, air drag only slightly affects the deflections of the bristles at practical rotating speeds.

To facilitate possible brush design work the problem was also studied employing a dimensionless formulation. The parameters that affect the magnitude of the normal force and the contact angle are five dimensionless numbers.

Keywords: Duct; Bristle; Normal force; Contact angle; Torque; Air drag; Dimensionless formulation

TABLE OF CONTENTS

NOMENCLATURE.....	4
1. INTRODUCTION.....	7
2. MODELING.....	10
3. SOLUTION METHOD.....	18
3.1 Discrete formulation	18
3.2 Solution details.....	22
4. DIMENSIONLESS FORMULATION	24
4.1 Manipulations.....	24
4.2 Dimensionless results.....	28
5. LABORATORY TEST	31
5.1 Experimental arrangement	31
5.2 Solution details.....	34
5.3 Additional test.....	38
6. RESULTS.....	41
6.1 Simulation details.....	41
6.2 Rotating bristle calculations.....	41
6.2.1 Deflection of rotating bristle.....	41
6.2.2 Dependence on the rotation speed of the bristle	43
6.2.3 Dependence on air drag.....	43
6.3 Results of laboratory test.....	46
6.3.1 Deflection of bristle	46
6.3.2 Magnitude of normal force	49
6.3.3 Magnitude of torque.....	50
6.3.4 Friction coefficient.....	50
6.4 Summary of the results.....	51
7. DISCUSSION	53
8. CONCLUSION	55
ACKNOWLEDGEMENTS	56
REFERENCES	57
APPENDIX.....	59

NOMENCLATURE

A	cross-sectional area of bristle
c	dimensionless multiplier
c_0, c_1, \dots, c_n	undetermined parameters
C_D	air drag coefficient
d	thickness of bristle
dm	mass element of bristle
ds	differential bristle length element
E	Young's modulus
El	flexural rigidity of bristle
L	length of bristle
L_1, L_2, \dots, L_m	Lagrangian interpolation functions
M	bending moment
M_1, M_2, \dots, M_j	first integrals of Lagrangian interpolation functions
N_1, N_2, \dots, N_j	second integrals of Lagrangian interpolation functions
n	rotation speed of bristle, degree of approximation, number of bristles
N	magnitude of normal force
P	cross-sectional normal force
q	air drag force per unit bristles length acting perpendicular to bristle
Q	shearing force
r	radial distance from origin to s
R	radius of duct
Re	Reynolds number = $\rho_a v d / \mu_a$
s	arc length coordinate of a generic point of bristle
s_1, s_2, \dots, s_m	interpolation points in interval $0 \leq s \leq L$
T	torque
W	weight
x, y	coordinates of a generic point of bristle
<i>Greek symbols</i>	
α	directed angle from initial ray
β	bristle tip contact angle
γ	angle between rod normal and rod velocity vector
θ	inclination angle of bristle axis with x -axis
$\tilde{\theta}$	approximation of θ
μ	kinetic coefficient of friction
μ_a	dynamic viscosity of air
ν_a	kinematic viscosity of air
ξ	ratio s/L

π_1	dimensionless number = $\rho AL^4 \omega^2 / EI$
π_2	dimensionless number = L/R
π_3	dimensionless number = μ
π_4	dimensionless number = $c^2 \rho_a L^5 \omega^2 d / EI$
π_5	dimensionless number = $c \rho_a \omega L d / \mu_a = c \omega L d / \nu_a$
ρ_a	density of air
ρ_b	density of bristle material
ϕ	inclination angle of a ray to s with respect to x -axis, polar angle
ω	angular speed of brush

Subscript

a	air
ad	air drag
b	bristle, bending
bf	bearing friction
c	centrifugal
fit	fitting polynomial function
N	air drag intensity normal to axis
$N\mu$	normal and friction force
s	simulated value

Superscript

–	dimensionless quantity
~	approximation of a quantity

Brackets

$\langle \ \rangle$	function of Reynolds number
---------------------	-----------------------------

1 INTRODUCTION

Dust and other contaminants accumulate on the surfaces of an air handling system during its construction and operation. Contaminated surfaces may increase energy consumption, decrease the airflow rate and cause malfunctions in the air handling system. Additionally, contamination into the supply air duct may cause problems for the occupants of the building. Therefore, the air handling system has to be cleaned regularly. In particular, those systems which convey high levels of dust or represent a fire hazard have to be cleaned frequently.

Mechanical brushing is an efficient method for cleaning air ducts [1]. Mechanical brushing systems consist of rotating brushes that detach particles from duct surfaces, cleaning devices to guide and rotate the brush into the duct, a low-pressure fan to convey the loosened particles from the duct, and a filter unit to remove particles as they pass through the filter. The brushes are guided into the ducts with flexible rods and normally rotate at speeds of $n = 300 - 1000$ rpm. The diameter of the brush is oversized compared to the diameter of the duct - i.e. the bristle length L duct radius R ratio is normally $1 < L/R < 1.3$. The thickness of the bristles d varies between 0.3 mm and 1.0 mm when fine, dry dust is removed. To date brushes have been designed using empirical methods. However, theoretical modelling offers a useful tool in development work for the use of brushes for different purposes.

The effect of varied parameters on the behaviour of rotating bristle was studied in references [2] and [3]. The results showed that the diameter of the bristle and the rotation speed strongly affect the magnitude of the bristle tip normal force N . With regard to the contact angle β , the bristle length duct radius ratio is the most important parameter. Air drag somewhat affects thin bristle behaviour at the rotation speeds of 300–1000 rpm that are used in practice. The rotation speed and the bristle length duct radius ratio are typical parameters that professional cleaners use to optimise brushes.

Compared to references [2] and [3], this report contains some new features, namely a dimensionless representation of the formulation and a description of an experimental test arrangement and a comparison of the results using the test and also using the

computational model. To make the report reasonably self-contained, the main assumptions and expressions from references [2] and [3] are repeated here.

Figure 1.1 (a) shows schematically the deformed shape of a typical rotating bristle in a duct and the forces acting at the bristle tip. We assume here that the rotation centre O situates at the geometric centre of a circular duct. The radius of the duct is denoted R and the length of the bristle L . The independent variable for the bristle shape description is taken to be the arc length s along the deformed bristle. Figure 1.1 (b) shows in more detail a possible scenario at the bristle tip.

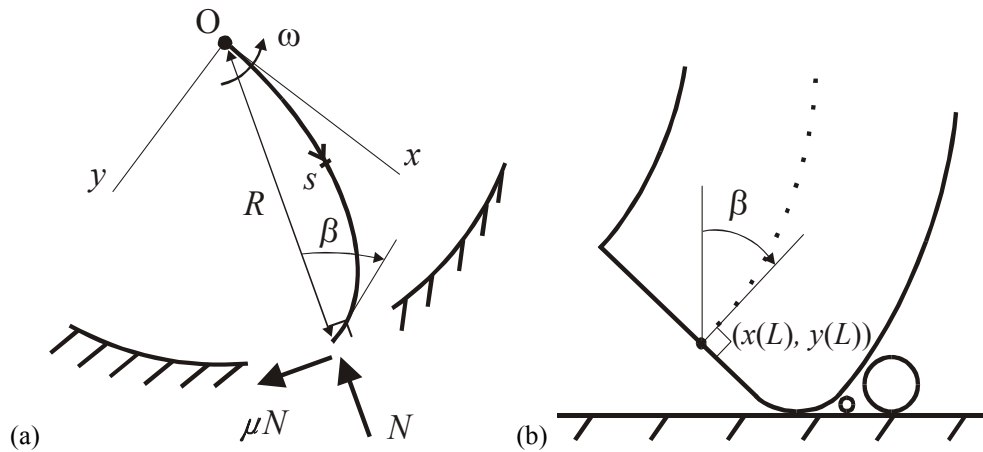


Fig. 1.1. (a) Deformed bristle and the contact forces at the bristle tip. (b) Bristle tip.

Of main interest is to determine the value of the unknown normal force N acting on the bristle tip, the contact angle β and torque T needed in terms of the parameters of the problem, such as the angular speed of the brush ω and the ratio L/R etc. The contact angle β is defined as the angle between the duct surface normal and the bristle axis tangent at the bristle tip (Figure 1.1). The larger the force μN , where μ is the friction coefficient, the better one would expect the cleaning efficiency to be. The effective value of μ may depend on β . Quantities N and β are thus obviously of importance in the cleaning process and it seems more or less clear that the larger the normal force and the smaller the contact angle the better the cleaning efficiency. In any case, this was one criterion used in looking at the results described in this report and in reference [2]. However, it is recognised that other factors such as the sweeping speed, the detailed geometric shape of the possibly worn bristle tip, the surface pressure, etc.

may also have influence on the cleaning efficiency. Theoretical and experimental work is needed to clarify the roles of N and β in the cleaning process.

2 MODELING

The bristle is modelled using large deformation elastic theory. Certain simplifying assumptions are made. First, plane steady motion of an initially straight uniform bristle is assumed. Second, zero size for the attaching frame is used. A correction for this would not be difficult. Third, air drag on the bristle somewhat decreases the contact force between a bristle tip and the duct surface [3]. However, air drag only slightly affects the deflection of the bristle at rotation speeds of 300–1000 rpm. A correction for air drag is taken into account and reference [3] describes in more detail the effect of air drag on the deflection of the single bristle. Fourth, the effect of gravity on the bristle is neglected. The order of the magnitude of the ratio $(2g/\omega^2 R)$ between the gravity of the bristle (mg) and the resulting approximate centrifugal force $(m\omega^2 R/2)$ is usually much below 0.2 with practical data. Fifth, the bristle is considered to obey elastic rod theory so that the deformations are due to the bending moment only and the deformations due to beam normal force and shearing force are neglected. This is well justified considering the slenderness of the bristles. Sixth, the contact forces are assumed to act at the central axis of the bristle tip which may lead to a small error (see Figure 1 (b)).

Figure 2.1 (a) describes the setting in some detail. The study of the bristle behaviour is performed in an xy -coordinate system with its origin at the rotation centre O and rotating with the attaching frame. The x -axis is along the undeformed straight bristle axis and the y -axis is 90 degrees in the clockwise direction according to the usual convention of the strength of materials, e.g. reference [4]. In this frame the bristle is assumed to be in a static state and the motion is taken into account in a well-known manner via centrifugal forces.

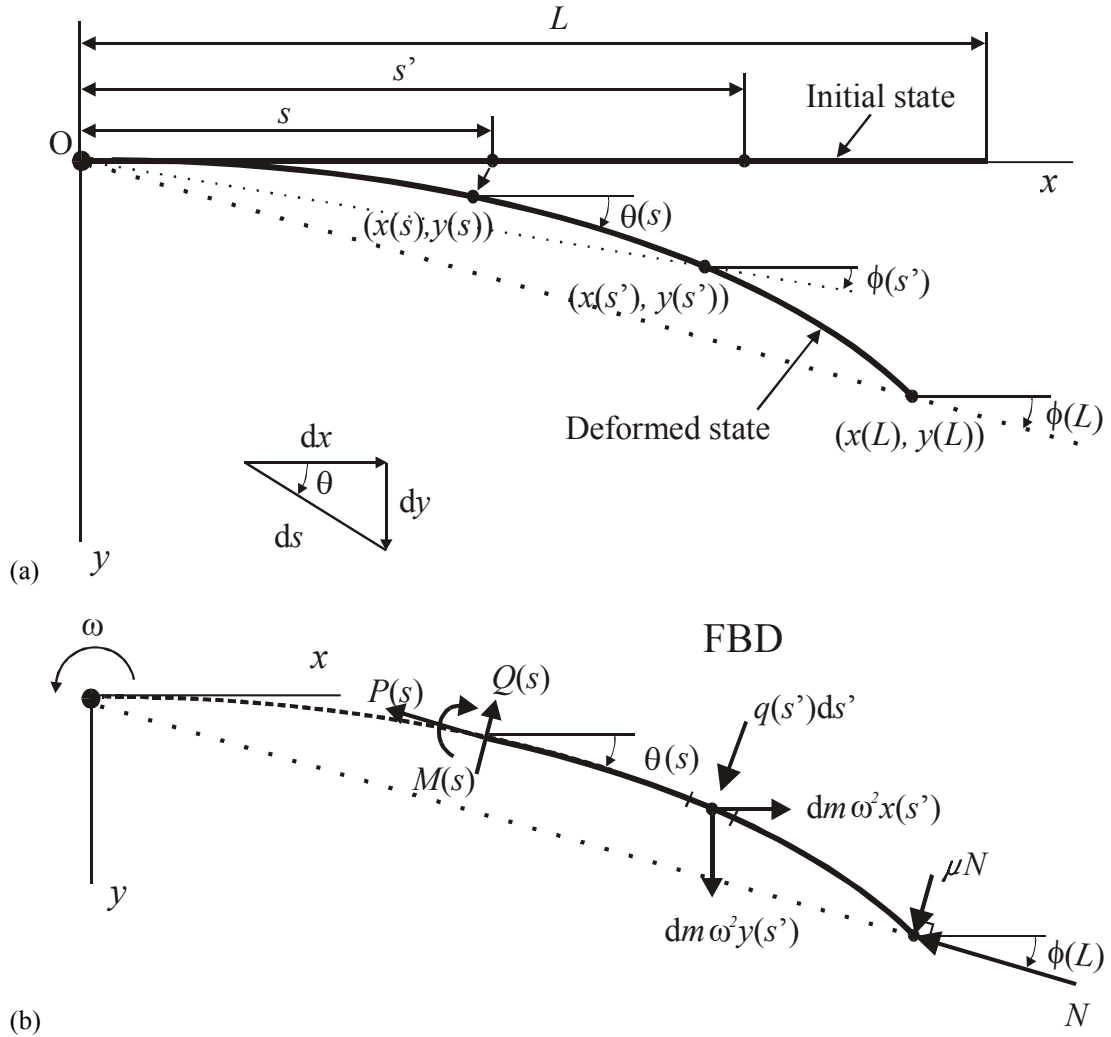


Fig. 2.1. (a) Large deflection of a deformed bristle and (b) a free-body diagram.

The exact differential equation of the deflection curve is [4]

$$M = -EI \frac{d\theta}{ds}. \quad (2.1)$$

Here θ is the inclination angle of the bristle axis with the x -axis, M the bending moment in the bristle, and EI the flexural rigidity of the bristle. Further, the shearing force Q is connected to the bending moment by $Q = dM/ds$ and thus with constant EI :

$$Q = -EI \frac{d^2\theta}{ds^2}. \quad (2.2)$$

Figure 2.1 (b) shows the free-body diagram of an end part of the bristle. In addition to the bending moment M and shearing force Q , the rod normal force P at the generic

rod cross-section is shown. A differential rod length element ds' has mass $dm = \rho A ds'$ where ρ is the density and A its cross-sectional area of the bristle. The centrifugal force components acting on mass element dm in the x - and y -directions are $dm\omega^2 x(s')$ and $dm\omega^2 y(s')$, respectively. The notation s' is used for an arc length coordinate referring to a generic point inside the end part of the bristle to differentiate it from the arc length coordinates referring to a generic cross-sectional point. Air drag is assumed to act perpendicular to the bristle axis. We thus neglect the possible axial component of the drag. Denoting the intensity by q [N/m], the force acting on ds' is in magnitude $q(s')ds'$. The inclination angle $\phi(L)$ at the bristle tip associated with the contact normal force N is fixed here due to the fact that the line of the action of the contact normal force N goes through the duct centre and thus here also through the rotation centre O . Assuming Coulomb friction, we obtain the friction force μN acting perpendicular to the contact normal force N . The equilibrium equation of the body in Figure 2.1 (b) in the direction of Q is

$$\begin{aligned}
Q - N \sin[\theta(s) - \phi(L)] - \mu N \cos[\theta(s) - \phi(L)] + \rho A \omega^2 \sin \theta(s) \int_s^L x(s') ds' \\
- \rho A \omega^2 \cos \theta(s) \int_s^L y(s') ds' - \int_s^L q(s') \cos[\theta(s') - \theta(s)] ds' = 0.
\end{aligned} \tag{2.3}$$

The shearing force expression is thus

$$Q = Q_{N\mu} + Q_c + Q_{ad} \tag{2.4}$$

with

$$\begin{aligned}
Q_{N\mu} &= N \sin[\theta(s) - \phi(L)] + \mu N \cos[\theta(s) - \phi(L)] \\
&= N [\sin \theta(s) \cos \phi(L) - \cos \theta(s) \sin \phi(L)] \\
&\quad + \mu N [\cos \theta(s) \cos \phi(L) + \sin \theta(s) \sin \phi(L)],
\end{aligned} \tag{2.5}$$

$$Q_c = -\rho A \omega^2 \sin \theta(s) \int_s^L x(s') ds' + \rho A \omega^2 \cos \theta(s) \int_s^L y(s') ds', \tag{2.6}$$

$$Q_{ad} = \int_s^L q(s') \cos[\theta(s') - \theta(s)] ds'$$

$$= \cos \theta(s) \int_s^L \cos \theta(s') q(s') ds' + \sin \theta(s) \int_s^L \sin \theta(s') q(s') ds'. \quad (2.7)$$

For clarity of later exposition and discussion, we have separated the shearing force Q into the contribution $Q_{N\mu}$ due to the normal contact force and friction, into the contribution Q_c due to the centrifugal forces and into the contribution Q_{ad} due to the air drag.

Substituting the shearing force expression (2.4) into (2.2) gives the governing field equation

$$Q \equiv Q_{N\mu} + Q_c + Q_{ad} = -EI \frac{d^2 \theta}{ds^2} \quad (2.8)$$

or in more detail

$$\begin{aligned} & N[\sin \theta(s) \cos \phi(L) - \cos \theta(s) \sin \phi(L)] + \mu N[\cos \theta(s) \cos \phi(L) + \sin \theta(s) \sin \phi(L)] \\ & - \rho A \omega^2 \sin \theta(s) \int_s^L x(s') ds' + \rho A \omega^2 \cos \theta(s) \int_s^L y(s') ds' \\ & + \cos \theta(s) \int_s^L \cos \theta(s') q(s') ds' + \sin \theta(s) \int_s^L \sin \theta(s') q(s') ds' = -EI \frac{d^2 \theta}{ds^2}. \end{aligned} \quad (2.9)$$

The boundary conditions are as follows. The bending moment must vanish at the bristle tip. This gives a force type condition

$$M(L) = 0, \quad (2.10)$$

or taking (2.1) into account, the condition

$$\frac{d\theta}{ds}(L) = 0. \quad (2.11)$$

The geometrical conditions are the following. At the origin the bristle axis is at a tangent to the x -axis:

$$\theta(0) = 0. \quad (2.12)$$

Further, the bristle tip with coordinates $x(L)$ and $y(L)$ is on the duct surface, i.e., its distance from the origin is R :

$$\sqrt{x^2(L) + y^2(L)} = R. \quad (2.13)$$

The problem to be solved is described by the field Eq. (2.9) and the boundary conditions (2.11) and (2.12). Additionally, there is the geometric constraint condition (2.13). The corresponding unknowns to be determined are the function $\theta = \theta(s)$ and the constant N .

Before proceeding, we have still to express x and y using θ . From Figure 2.1 (a)

$$\cos \theta(s) = \frac{dx}{ds}, \quad (2.14)$$

$$\sin \theta(s) = \frac{dy}{ds}. \quad (2.15)$$

Integration gives

$$x(s) = \int_0^s \cos \theta(s') ds', \quad (2.16)$$

$$y(s) = \int_0^s \sin \theta(s') ds'. \quad (2.17)$$

Using these in (2.9), we write

$$x(s') = \int_0^{s'} \cos \theta(s^*) ds^*, \quad (2.18)$$

$$y(s') = \int_0^{s'} \sin \theta(s^*) ds^*. \quad (2.19)$$

The additional notation s^* has been used in an effort to differentiate the two integration variables from each other. Finally, at the bristle tip

$$x(L) = \int_0^L \cos \theta(s') ds', \quad (2.20)$$

$$y(L) = \int_0^L \sin \theta(s') ds'. \quad (2.21)$$

From Figure 2.1 (a), we also have the relations

$$\cos \phi(L) = \frac{x(L)}{R}, \quad (2.22)$$

$$\sin \phi(L) = \frac{y(L)}{R} \quad (2.23)$$

to be used in (2.9).

Air resistance is considered next in more detail. The standard form of magnitude of the air drag per unit length for a cylinder with circular cross-section is [5]

$$q_N = \frac{1}{2} C_D \rho_a v^2 d, \quad (2.24)$$

where C_D is the air drag coefficient, ρ_a the density of air, v the speed of the cylinder with respect to air and d the diameter of the cylinder. The drag coefficient depends on the Reynolds number

$$\text{Re} = \frac{\rho_a v d}{\mu_a}, \quad (2.25)$$

where μ_a is the viscosity of the air. The speed of a bristle point with respect to stagnant air is $\omega r(s')$, where

$$r(s') = \sqrt{x^2(s') + y^2(s')} \quad (2.26)$$

is the radial distance from the origin. The brush certainly sets the air around into motion which is difficult to estimate. In an effort to take this into account we evaluate the speed by

$$v = c \omega r(s'), \quad (2.27)$$

where c is a dimensionless multiplier ($0 < c \leq 1$). If some experimental results are available, c can hopefully be made use of. According to [6], when the flow is inclined to the axis of a cylinder, the air drag intensity normal to the axis can be evaluated from

$$q = q_N \cos^2 \gamma, \quad (2.28)$$

where

$$\gamma(s') = \theta(s') - \phi(s') \quad (2.29)$$

is here the angle between the rod normal and rod velocity vector. In more detail,

$\cos \gamma(s') = \cos \theta(s') \cos \phi(s') + \sin \theta(s') \sin \phi(s')$ and

$$\cos \phi(s') = \frac{x(s')}{r(s')}, \quad (2.30)$$

$$\sin \phi(s') = \frac{y(s')}{r(s')}. \quad (2.31)$$

The air drag coefficient is evaluated by fitting a fourth degree polynomial function for a circular cylinder from measured data [5] as a function of the Reynolds number in logarithmic coordinates in the form $\log C_D = f(\log \text{Re})$. This gives

$$C_D = 10^{1.005 - 0.614 \log \text{Re} + 0.166 (\log \text{Re})^2 - 0.037 (\log \text{Re})^3 + 0.04819 (\text{Re})^4}. \quad (2.32)$$

The graph of (2.32) is shown in Figure 2.2. Expression (2.32) should not be used if the Reynolds number exceeds 10^4 because of the non-smooth behaviour of C_D around this point. In this application this limit was not exceeded.

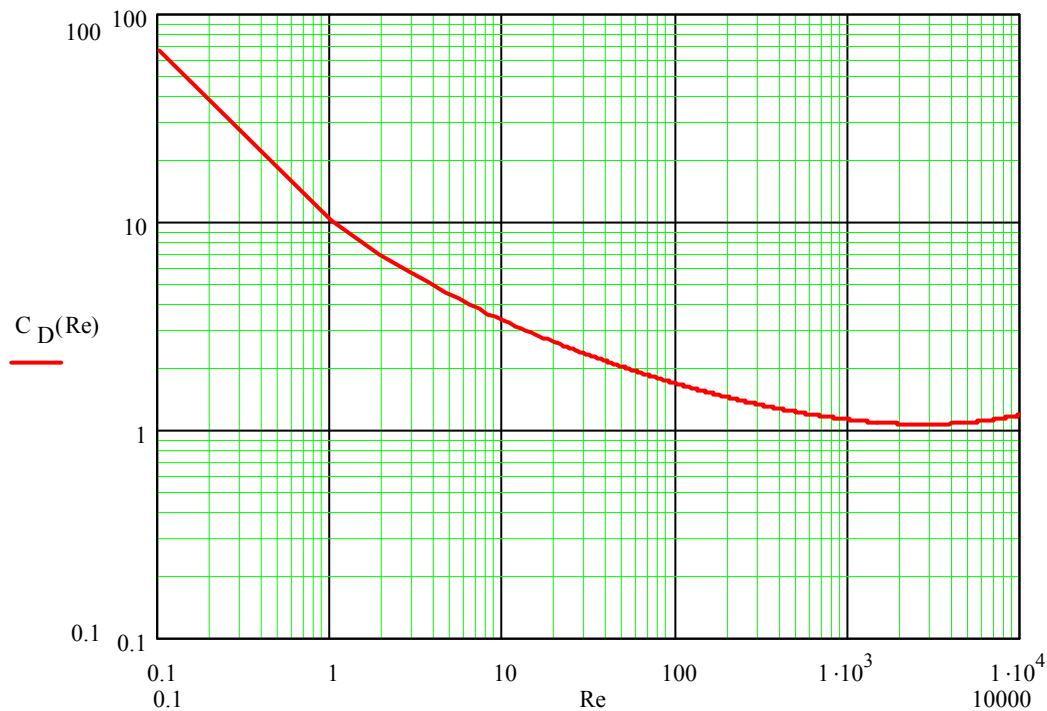


Fig. 2.2. Fitting a fourth degree polynomial function for circular cylinders as a function of the Reynolds number in logarithmic coordinates.

It is quite clearly not possible to find an analytical closed form solution for the present problem. The discrete version of the model which can be solved numerically is presented next.

3 SOLUTION METHOD

3.1 Discrete formulation

The unknown function $\theta = \theta(s)$ to be determined is approximated by a trial solution

$$\theta(s) \approx \tilde{\theta}(s) = \sum_{i=0}^n c_i s^i = c_0 + c_1 s + c_2 s^2 + c_3 s^3 + \dots + c_n s^n, \quad (3.1)$$

where c_0, c_1, \dots, c_n are undetermined parameters and the given basis functions are simply powers of s . In the numerical applications we have selected $n = 6$. Thus the problem of determining the function $\theta = \theta(s)$ and the constant N is transformed to the determination of the eight unknown constants $c_0, c_1, c_2, c_3, c_4, c_5, c_6, N$. We have to generate eight (or more) algebraic equations for this purpose. Three of the equations come from the conditions (2.11), (2.12) and (2.13). The remaining five are obtained from the field Eq. (2.9) by applying the point collocation method with five collocation points situated uniformly at $s_1 = 0, s_2 = L/4, s_3 = L/2, s_4 = 3L/4, s_5 = L$. The point collocation method is the simplest criterion for determining the undetermined parameters in connection with the method of weighted residuals [7]. The detailed final equations are developed and solved with the Mathcad program [8] given in the Appendix. The code, with additional comments, is available on the Mathcad web site [9].

The first and second derivatives of $\tilde{\theta}(s)$ needed in (2.9) and (2.11) are simply

$$\frac{d\tilde{\theta}}{ds} = \sum_{i=1}^n i c_i s^{i-1} = c_1 + 2c_2 s + 3c_3 s^2 + \dots, \quad (3.2)$$

and

$$\frac{d^2\tilde{\theta}}{ds^2} = \sum_{i=2}^n i(i-1)c_i s^{i-2} = 2c_2 + 6c_3 s + \dots \quad (3.3)$$

The equivalents of formulas (2.16) and (2.17) would give here

$$\tilde{x}(s) = \int_0^s \cos \tilde{\theta}(s') ds', \quad (3.4)$$

$$\tilde{y}(s) = \int_0^s \sin \tilde{\theta}(s') ds'. \quad (3.5)$$

However, a closed form integration using (3.1) does not seem possible. We therefore approximate the integrands first using Lagrangian interpolation [10]:

$$\cos[\tilde{\theta}(s')] \approx \sum_{j=1}^m L_j(s') \cos \tilde{\theta}(s'_j), \quad (3.6)$$

$$\sin[\tilde{\theta}(s')] \approx \sum_{j=1}^m L_j(s') \sin \tilde{\theta}(s'_j). \quad (3.7)$$

Here $L_j(s')$ are the Lagrangian interpolation functions and the coordinates s'_j refer to the interpolation points where the cosines and sines are evaluated:

$$\cos[\tilde{\theta}(s'_j)] \approx \cos[c_0 + c_1 s'_j + c_2 (s'_j)^2 + c_3 (s'_j)^3 \dots], \quad (3.8)$$

$$\sin[\tilde{\theta}(s'_j)] \approx \sin[c_0 + c_1 s'_j + c_2 (s'_j)^2 + c_3 (s'_j)^3 \dots]. \quad (3.9)$$

Using (3.6) and (3.7), the integrals are easily evaluated as the Lagrangian interpolation functions are polynomials. The results are

$$\tilde{x}(s) = \sum_{j=1}^m M_j(s) \cos[\tilde{\theta}(s'_j)], \quad (3.10)$$

$$\tilde{y}(s) = \sum_{j=1}^m M_j(s) \sin[\tilde{\theta}(s'_j)], \quad (3.11)$$

where

$$M_j(s) = \int_0^s L_j(s') ds'. \quad (3.12)$$

In addition, to evaluate the centrifugal terms, we need the integrals

$$\int_s^L \tilde{x}(s') ds' = \int_0^L \tilde{x}(s') ds' - \int_0^s \tilde{x}(s') ds' = \sum_{j=1}^m [N_j(L) - N_j(s)] \cos[\tilde{\theta}(s'_j)], \quad (3.13)$$

$$\int_s^L \tilde{y}(s') ds' = \int_0^L \tilde{y}(s') ds' - \int_0^s \tilde{y}(s') ds' = \sum_{j=1}^m [N_j(L) - N_j(s)] \sin[\tilde{\theta}(s'_j)], \quad (3.14)$$

where

$$N_j(s) = \int_0^s M_j(s') ds'. \quad (3.15)$$

In the numerical calculations we have taken $m=4$ and the interpolation points uniformly so that $s_1' = 0$, $s_2' = L/3$, $s_3' = 2L/3$, $s_4' = L$ in the interval $0 \leq s \leq L$. As examples, functions L_1 , L_2 and M_1 , M_2 and N_1 , N_2 are shown in Figure 3.1 as functions of $\xi = s'/L$ or $\xi = s/L$.

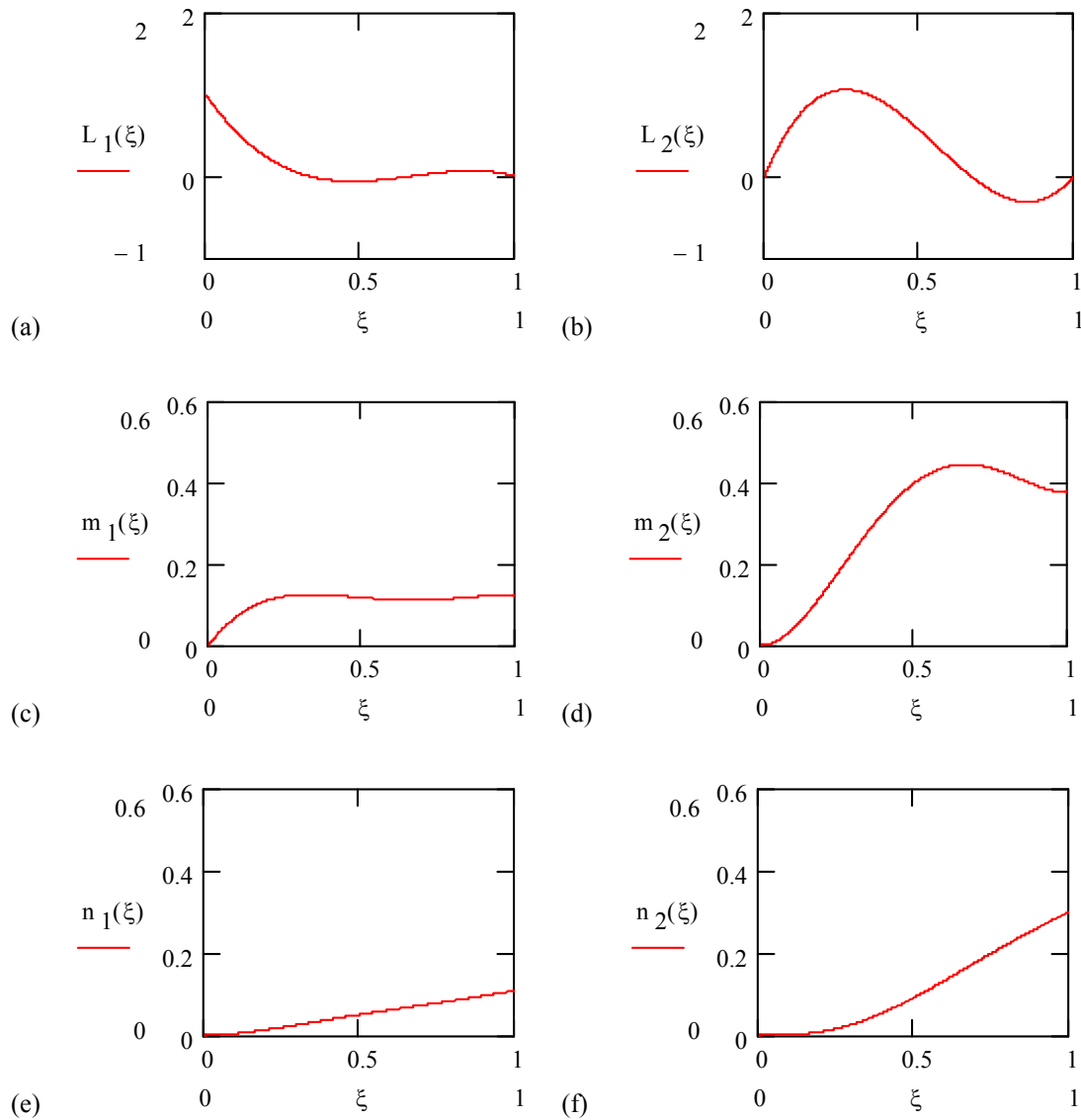


Fig. 3.1. Lagrangian interpolation functions (a) L_1 and (b) L_2 , their first integrals (c) $m_1 = M_1/L$ and (d) $m_2 = M_2/L$ and their second integrals (e) $n_1 = N_1/L^2$ and (f) $n_2 = N_2/L^2$ as functions of ξ .

In detail,

$$L_1(s) = \frac{-9}{2L^3}s^3 + \frac{9}{L^2}s^2 - \frac{11}{2L}s + 1, \quad (3.16)$$

$$L_2(s) = \frac{27}{2L^3}s^3 - \frac{45}{2L^2}s^2 + \frac{9}{L}s, \quad (3.17)$$

$$M_1(s) = \frac{-9}{8L^3}s^4 + \frac{3}{L^2}s^3 - \frac{11}{4L}s^2 + s, \quad (3.18)$$

$$M_2(s) = \frac{27}{8L^3}s^4 - \frac{15}{2L^2}s^3 + \frac{9}{2L}s^2, \quad (3.19)$$

$$N_1(s) = \frac{-9}{40L^3}s^5 + \frac{3}{4L^2}s^4 - \frac{11}{12L}s^3 + \frac{s^2}{2}, \quad (3.20)$$

$$N_2(s) = \frac{27}{40L^3}s^5 - \frac{15}{8L^2}s^4 + \frac{3}{2L}s^3. \quad (3.21)$$

The five discrete equations following from (2.9) using collocation are thus

$$\begin{aligned} & \tilde{N} \left[\sin \tilde{\theta}(s_k) \frac{\tilde{x}(L)}{R} - \cos \tilde{\theta}(s_k) \frac{\tilde{y}(L)}{R} \right] + \mu \tilde{N} \left[\cos \tilde{\theta}(s_k) \frac{\tilde{x}(L)}{R} + \sin \tilde{\theta}(s_k) \frac{\tilde{y}(L)}{R} \right] \\ & - \rho A \omega^2 \sin \tilde{\theta}(s_k) \int_{s_k}^L \tilde{x}(s') ds' + \rho A \omega^2 \cos \tilde{\theta}(s_k) \int_{s_k}^L \tilde{y}(s') ds' \\ & \cos \tilde{\theta}(s_k) \int_{s_k}^L \cos \tilde{\theta}(s') q(s') ds' + \sin \tilde{\theta}(s_k) \int_{s_k}^L \sin \tilde{\theta}(s') q(s') ds' \\ & = -EI \frac{d^2 \tilde{\theta}}{ds^2}(s_k), \quad k = 1, \dots, 5. \end{aligned} \quad (3.22)$$

Further, we have to apply in detail (3.1), (3.3), (3.10), (3.11) and (3.13), (3.14). In addition, evaluation of the terms due to $q(s')$ is rather complex, as is described below.

The resulting equations are strongly nonlinear in the coefficients c_i .

Discretization of the boundary conditions is simple. Condition (2.12) leads to

$$\tilde{\theta}(0) = c_0 = 0. \quad (3.23)$$

Condition (2.11) leads to

$$\frac{d\tilde{\theta}}{ds}(L) = c_1 + 2c_2L + 3c_3L^2 + \dots = 0. \quad (3.24)$$

These are both linear. Finally, (2.13) gives

$$\sqrt{\tilde{x}^2(L) + \tilde{y}^2(L)} = R, \quad (3.25)$$

where (3.10) and (3.11) have to be applied again with $s = L$.

3.2 Solution details

The resulting non-linear algebraic system consisting of the eight Eqs. (3.22), (3.23), (3.24) and (3.25) was solved by the Mathcad program. The program needs an initial guess for the unknown to proceed. The initial values were taken to be, $c_0 = 0$, $c_1 = 0.5/L$, $c_2 = -0.25/L^2$, $c_3 = c_4 = c_5 = c_6 = 0$ and $N = 0$. (Parameter c_0 was not actually included in the code as its value is determined in advance by (3.23).) The non-zero values were estimated making some use of Eqs. (2.11) and (2.21). The final program gave apparently convergent solutions in all of the cases studied. However, with higher rotation speeds some updating of the constants from the results with lower speeds were needed.

With regard to the integrals in Eq. (3.22), the terms due to centrifugal forces have been evaluated "directly", as is explained above. However, the terms from air drag are so complicated that a direct approach is out of the question. Thus $q(s')$ is updated iteratively according to the current achieved shape (c_0, c_1, \dots, c_n) of the bristle. The integrands $\cos\tilde{\theta}(s')q(s')$ and $\sin\tilde{\theta}(s')q(s')$ are then represented by the Lagrangian interpolation functions and integrated analytically. This is an "indirect" approach, which could also actually be used for the centrifugal forces. On average about three iterations were needed to achieve practically converged results.

In references [2, 11] a somewhat similar problem – the famous Elastica problem described in reference [4] – with a known analytical solution is studied using the calculation model. The results of this preliminary calculation using the discrete method may be viewed as surprisingly accurate taking into account the seemingly rather crude

approximation. Thus we may have some confidence in using the discrete formulation to approximate the rotating bristle in the duct.

4 DIMENSIONLESS FORMULATION

4.1 Manipulations

To simplify the study of the dependencies between the various quantities we employ here a dimensionless formulation. The final purpose of this presentation is to make the eventual future design process as systematic as possible. As is mentioned in [7]: "This is an extremely useful organizational tool of the analyst. In connection with numerical calculations it removes all unnecessary symbols, leaving the basic problem in its simplest form."

Using the dimensionless coordinate

$$\xi = \frac{s}{L}, \quad \xi \in [0,1], \quad (4.1)$$

we obtain

$$\frac{d(\cdot)}{ds} = \frac{1}{L} \frac{d(\cdot)}{d\xi}, \quad \frac{d^2(\cdot)}{ds^2} = \frac{1}{L^2} \frac{d^2(\cdot)}{d\xi^2}, \quad (4.2)$$

$$\int_s^L (\cdot) ds = L \int_{\xi}^1 (\cdot) d\xi, \quad \int_0^L (\cdot) ds = L \int_0^1 (\cdot) d\xi. \quad (4.3)$$

Dependent variable θ is already dimensionless. We denote $\bar{\theta}(\xi) \equiv \theta(s(\xi))$. We also denote

$$\bar{x} = \frac{x}{L}, \quad \bar{y} = \frac{y}{L}. \quad (4.4)$$

Eqs. (2.2), (2.11), (2.12) and (2.13) become first

$$Q + EI \frac{1}{L^2} \frac{d^2 \bar{\theta}}{d\xi^2} = 0, \quad 0 < \xi < 1, \quad (4.5)$$

$$\frac{1}{L} \frac{d\bar{\theta}}{d\xi}(1) = 0, \quad (4.6)$$

$$\bar{\theta}(0) = 0, \quad (4.7)$$

$$L\sqrt{\bar{x}^2(1) + \bar{y}^2(1)} = R \quad (4.8)$$

and after some arrangement

$$\frac{d^2\bar{\theta}}{d\xi^2} + \frac{L^2}{EI}Q = 0, \quad 0 < \xi < 1, \quad (4.9)$$

$$\frac{d\bar{\theta}}{d\xi}(1) = 0, \quad (4.10)$$

$$\bar{\theta}(0) = 0, \quad (4.11)$$

$$\sqrt{\bar{x}^2(1) + \bar{y}^2(1)} = \frac{R}{L}. \quad (4.12)$$

It is seen that functions such as $\bar{x}(\xi) = x(s(\xi))/L$ depend in a complicated manner on function $\bar{\theta}(\xi)$. For instance as

$$\begin{aligned} x(s) &= \int_0^s \cos \theta(s') ds' \\ &= L \int_0^\xi \cos \bar{\theta}(\xi') d\xi', \end{aligned} \quad (4.13)$$

we obtain

$$\bar{x}(\xi) = \int_0^\xi \cos \bar{\theta}(\xi') d\xi'. \quad (4.14)$$

Thus, in the following, to avoid very complicated expressions, we do not show in detail some of the dependencies of say \bar{x} and \bar{y} on $\bar{\theta}$.

The term (2.5):

$$\begin{aligned} Q_{N\mu} &= N[\sin \theta(s)\cos \phi(L) - \cos \theta(s)\sin \phi(L)] \\ &+ \mu N[\cos \theta(s)\cos \phi + \sin \theta(s)\sin \phi(L)] \\ &= N[\sin \bar{\theta}(\xi)\cos \bar{\phi}(1) - \cos \bar{\theta}(\xi)\sin \bar{\phi}(1)] \\ &+ \mu N[\cos \bar{\theta}(\xi)\cos \bar{\phi}(1) + \sin \bar{\theta}(\xi)\sin \bar{\phi}(1)]. \end{aligned} \quad (4.15)$$

The term (2.6):

$$Q_c = -\rho A \omega^2 \sin \theta(s) \int_s^L x(s') ds' + \rho A \omega^2 \cos \theta(s) \int_s^L y(s') ds'$$

$$\begin{aligned}
&= -\rho A \omega^2 \sin \bar{\theta}(\xi) L^2 \int_{\xi}^1 \bar{x}(\xi') d\xi' + \rho A \omega^2 \cos \bar{\theta}(\xi) L^2 \int_s^L \bar{y}(\xi') d\xi' \\
&= -\rho A L^2 \omega^2 \sin \bar{\theta}(\xi) \int_{\xi}^1 \bar{x}(\xi') d\xi' + \rho A L^2 \omega^2 \cos \bar{\theta}(\xi) \int_s^L \bar{y}(\xi') d\xi'. \tag{4.16}
\end{aligned}$$

The term (2.7):

$$\begin{aligned}
Q_{\text{ad}} &= \cos \theta(s) \int_s^L \cos \theta(s') q(s') ds' + \sin \theta(s) \int_s^L \sin \theta(s') q(s') ds' \\
&= \cos \bar{\theta}(\xi) L \int_{\xi}^1 \cos \bar{\theta}(\xi') \bar{q}(\xi') d\xi' + \sin \bar{\theta}(\xi) L \int_s^L \sin \bar{\theta}(\xi') \bar{q}(\xi') d\xi', \tag{4.17}
\end{aligned}$$

where we have denoted $\bar{q}(\xi') = q(s(\xi'))$ demands some more detailed considerations.

From (2.24), (2.27), (2.28),

$$q(s') = \frac{1}{2} C_D \rho_a [c \omega r(s')]^2 d \cos^2 \gamma(s') \tag{4.18}$$

and dependence in the drag coefficient is of the form

$$C_D = C_D \langle \text{Re} \rangle = C_D \left\langle \frac{\rho_a c \omega r(s') d}{\mu_a} \right\rangle. \tag{4.19}$$

We have used here the notation $\langle \rangle$ to emphasize the dependency and to avoid possible confusion with mere multiplication.

Denoting $\bar{r} = r/L$, $\bar{\gamma}(\xi') = \gamma(s(\xi'))$, we obtain

$$\begin{aligned}
\bar{q}(\xi') &= \frac{1}{2} C_D \left\langle \frac{\rho_a c \omega L \bar{r}(\xi') d}{\mu_a} \right\rangle \rho_a c^2 \omega^2 L^2 \bar{r}^2(\xi') d \cos^2 \bar{\gamma}(\xi') \\
&= \frac{1}{2} c^2 \rho_a \omega^2 L^2 d C_D \left\langle \frac{c \rho_a \omega L d}{\mu_a} \bar{r}(\xi') \right\rangle \bar{r}^2(\xi') \cos^2 \bar{\gamma}(\xi'). \tag{4.20}
\end{aligned}$$

Substituting this in (4.17) gives

$$\begin{aligned}
Q_{\text{ad}} &= \frac{1}{2} c^2 \rho_a \omega^2 L^3 d \left[\cos \bar{\theta}(\xi) \int_{\xi}^1 \cos \bar{\theta}(\xi') C_D \left\langle \frac{c \rho_a \omega L d}{\mu_a} \bar{r}(\xi') \right\rangle \bar{r}^2(\xi') \cos^2 \bar{\gamma}(\xi') d\xi' \right] \\
&\quad + \frac{1}{2} c^2 \rho_a \omega^2 L^3 d \left[\sin \bar{\theta}(\xi) \int_{\xi}^1 \sin \bar{\theta}(\xi') C_D \left\langle \frac{c \rho_a \omega L d}{\mu_a} \bar{r}(\xi') \right\rangle \bar{r}^2(\xi') \cos^2 \bar{\gamma}(\xi') d\xi' \right]. \tag{4.21}
\end{aligned}$$

We next define a dimensionless normal force

$$\bar{N} = \frac{L^2}{EI} N = \frac{64}{\pi} \frac{L^2}{Ed^4} N. \quad (4.22)$$

Multiplying the shearing force contributions by the factor L^2/EI and substituting the results in (4.9) gives the final dimensionless field equation

$$\begin{aligned} \frac{d^2 \bar{\theta}}{d\xi^2} + \bar{N} [\sin \bar{\theta}(\xi) \cos \bar{\phi}(1) - \cos \bar{\theta}(\xi) \sin \bar{\phi}(1)] + \mu \bar{N} [\cos \bar{\theta}(\xi) \cos \bar{\phi}(1) + \sin \bar{\theta}(\xi) \sin \bar{\phi}(1)] \\ - \frac{\rho AL^4 \omega^2}{EI} \sin \bar{\theta}(\xi) \int_{\xi}^1 \bar{x}(\xi') d\xi' + \frac{\rho AL^4 \omega^2}{EI} \cos \bar{\theta}(\xi) \int_{\xi}^1 \bar{y}(\xi') d\xi' \\ + \frac{1}{2} \frac{c^2 \rho_a \omega^2 L^5 d}{EI} \left[\cos \bar{\theta}(\xi) \int_{\xi}^1 \cos \bar{\theta}(\xi') C_D \left\langle \frac{c \rho_a \omega L d}{\mu_a} \bar{r}(\xi') \right\rangle \bar{r}^2(\xi') \cos^2 \bar{\gamma}(\xi') d\xi' \right] \\ + \frac{1}{2} \frac{c^2 \rho_a \omega^2 L^5 d}{EI} \left[\sin \bar{\theta}(\xi) \int_{\xi}^1 \sin \bar{\theta}(\xi') C_D \left\langle \frac{c \rho_a \omega L d}{\mu_a} \bar{r}(\xi') \right\rangle \bar{r}^2(\xi') \cos^2 \bar{\gamma}(\xi') d\xi' \right] = 0. \end{aligned} \quad (4.23)$$

For a circular cross-section with diameter d

$$A = \frac{\pi d^2}{4}, \quad I = \frac{\pi d^4}{64} \quad (4.24)$$

and

$$\frac{\rho AL^4 \omega^2}{EI} = 16 \frac{\rho L^4 \omega^2}{Ed^2} = 16 \left(\frac{L}{d} \right)^2 \frac{\rho L^2 \omega^2}{E}. \quad (4.25)$$

Observing the governing dimensionless formulation consisting of the field Eq. (4.23) and of the conditions (4.10), (4.11), (4.12) shows that solution $\bar{\theta}(\xi)$, \bar{N} depends on five dimensionless numbers:

$$\pi_1 = \frac{\rho AL^4 \omega^2}{EI}, \quad (4.26)$$

$$\pi_2 = \frac{L}{R}, \quad (4.27)$$

$$\pi_3 = \mu, \quad (4.28)$$

$$\pi_4 = \frac{c^2 \rho_a \omega^2 L^5 d}{EI}, \quad (4.29)$$

$$\pi_5 = \frac{c\rho_a\omega Ld}{\mu_a} = \frac{c\omega Ld}{v_a}. \quad (4.30)$$

Knowledge of these dependencies is made use of in representation of numerical results next.

4.2 Dimensionless results

Figures 4.1–4.3 present the magnitude of the dimensionless normal force \bar{N} and the contact angle β as a function of the dimensionless numbers $\pi_1 = \rho AL^4 \omega^2 / EI$, $\pi_2 = L/R$ and $\pi_3 = \mu$.

In Figure 4.1 the magnitude of the dimensionless normal force and the contact angle are shown as functions of the dimensionless number π_1 .

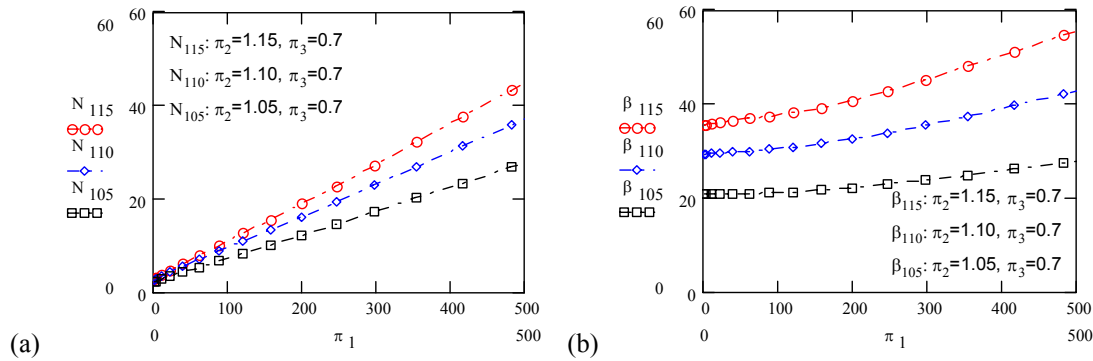


Fig. 4.1. (a) The dimensionless normal force \bar{N} [-] and (b) contact angle β [°] as functions of π_1 .

The normal force increases roughly linearly when π_1 changes from 0 to 500 which covers the normally used range in rotating brush duct cleaning. The centrifugal forces grow quadratically with the angular speed ω . Thus one could initially expect \bar{N} to grow linearly with $\pi_1 = \rho AL^4 \omega^2 / EI$ as seems to be the case in Figure 4.1 (a). However, as π_1 is higher than 4000, which is an unrealistic π_1 value, the magnitude of the normal force only increases slowly. This is probably explainable by the changing shape of the bristle so that the centrifugal force components have "changing lines of actions" when the rotation speed increases. As is to be expected, the magnitude of the normal force and the contact angle increase when parameter π_2 grows.

Figure 4.2 presents the magnitude of the dimensionless normal force and the contact angle as functions of the dimensionless number π_2 .

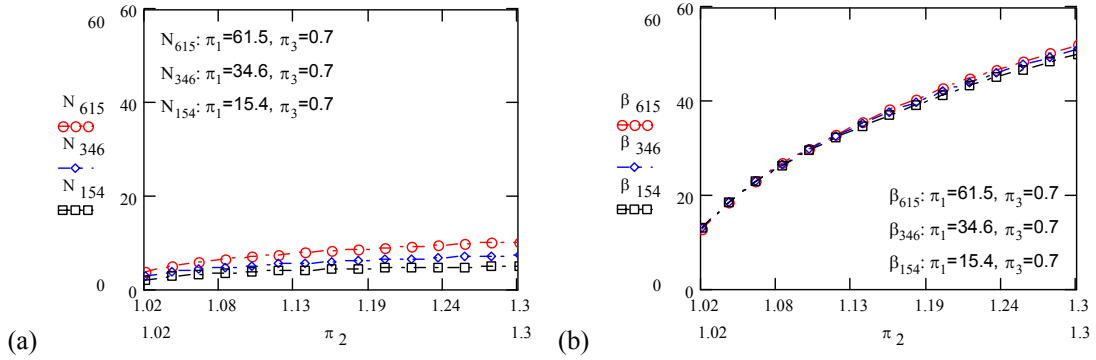


Fig. 4.2. (a) The dimensionless normal force \bar{N} [-] and (b) contact angle β [°] as functions of π_2 .

Both the magnitude of the normal force and the contact angle increase roughly quadratically as a function of $\pi_2 = L/R$. With higher values of π_2 the bristle "has to bend more to fit in the duct" so the results seem to be intuitively correct. The magnitude of the normal force and the contact angle increase when parameter π_1 grows. The values of π_1 15.4, 34.6 and 61.5 correspond to the rotation speeds of 500, 750 and 1000 rpm with the parameters values presented in Chapter 6.1 (except Young's modulus value $E = 2$ GPa).

Figure 4.3 presents the magnitude of the dimensionless normal force and the contact angle as functions of π_3 .

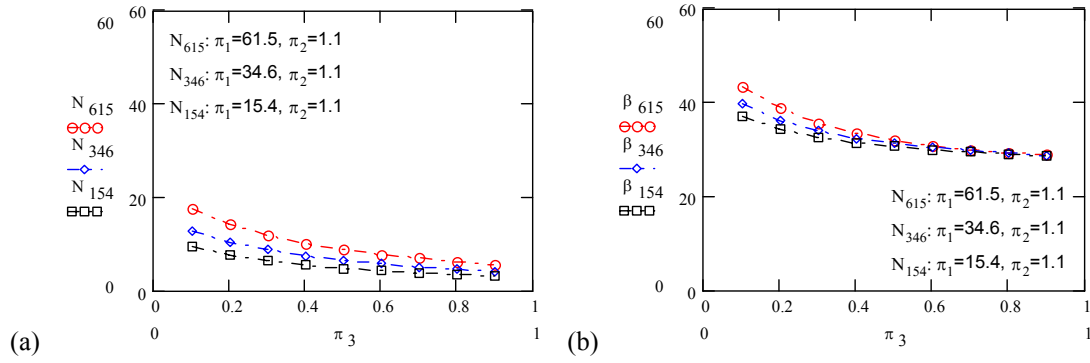


Fig. 4.3. (a) The dimensionless normal force \bar{N} [-] and (b) contact angle β [$^\circ$] as functions of π_3 .

The growth of the dimensionless number $\pi_3 = \mu$ acts in an opposite manner to π_1 and π_2 to the magnitude of the normal force and the contact angle. The decrease of the normal force with increasing π_3 seems plausible as the friction force has a direction with "large bending influence". To achieve high normal contact force, π_3 should be low.

In practice, dimensionless numbers π_1 and π_2 are the parameters that professional cleaners can use to optimise the duct cleaning brush. In rotating brush duct cleaning the common range of π_1 and π_2 are $0 < \pi_1 < 100$ and $1 < \pi_2 < 1.3$, respectively. The manufactures of the brushes can affect π_3 by selecting a suitable material property for the bristle. According to reference [3], air drag does not affect thin bristle behaviour strongly at practical rotation speeds and, therefore, dependencies on the dimensionless numbers π_4 and π_5 are not considered in this report.

5 LABORATORY TEST

5.1 Experimental arrangement

A rotating brush was tested in the Laboratory for Heating Ventilating and Air-Conditioning at Helsinki University of Technology. A round duct with a diameter $2R = 0.315$ m was prepared from a metal sheet plate with a width of 0.2 m. The diameter $2L$ of the tested brush was 0.35 m and the bristles were nylon ($d = 1 \times 10^{-3}$ m). The bristles were connected on a spiral frame made of metal wire. The number of bristles n was approximately 1000. The brush was centralized at the centre of the duct with the shaft of an electric motor (0.55 kW). In addition, certain tests were performed with just a single pair of bristles. Figure 5.1 presents some details of the instrumentation of the laboratory test.



Fig. 5.1. Experimental arrangement in the laboratory.

Measurements were obtained using force transducers 1, 2, 3 and 4. The range of transducers 1 and 4 were 0–118 N and for transducers 2 and 3 0–29 N. The transducers were located as indicated in Figures 5.1 and 5.2. The purposes of

transducers 1 and 4 were to determine the torque (twisting moment) from the contact friction and the output torque from the electric motor, respectively. The purpose of transducers 2 and 3 was to additionally measure the "opening force" in the seam of the duct frame at the left-hand side. The output torque T from the motor is considered to be balanced in general by the torque T_{bf} due to the bearing friction (some possible air drag acting on the shaft is included), by the torque T_{ad} due to the air drag from the brush (or from a bristle pair) and by the torque T_{μ} due to the contact friction of the brush (or of a bristle pair) with the duct surface; thus in general $T = T_{bf} + T_{ad} + T_{\mu}$. The motor output torque is obtained from

$$T = Pb, \quad (5.1)$$

where P (positive when transducer 4 is in tension) is the force measured by transducer 4 and $b = 0.227$ m is the horizontal distance between the centroid of the motor shaft and transducer 4 (Figure 5.2). Torque T_{bf} for a given rotation speed is obtained by rotating the motor alone, so then $T_{bf} = T$. When the brush rotates with contact, the total output torque $T = T_{bf} + T_{ad} + T_{\mu}$. Assuming T_{bf} is known for a given rotation speed, we can then determine $T_{ad} + T_{\mu} = T - T_{bf}$ from the experiment. Further, T_{μ} can be obtained using transducer 1 as is described below from Eq. (5.15), so finally we can determine T_{ad} from

$$T_{ad} = (T - T_{bf})_4 - (T_{\mu})_1, \quad (5.2)$$

where the meaning of the notations is obvious.

To have some estimate of the effect of air drag without the inclusion of contact forces, torque due to air drag was measured separately by rotating the brush in "air", meaning that the duct was removed. In addition, the brush was rotated without contact in a duct with a diameter of 0.365 m. Here $T = T_{bf} + T_{ad}$ and we can determine T_{ad} assuming again T_{bf} is known for a given rotation speed. However, this torque

$$T_{ad} = T - T_{bf} \quad (5.3)$$

is naturally not the same as the torque T_{ad} obtained by (5.2) with a brush in contact with the duct. Reference [3] presents the effect of the air drag on the torque by using Eqs. (5.1)–(5.3).

Further, experiments were performed using single pairs of bristles without trying to employ the transducers as the forces involved would be too small for proper measurements. Instead, bristle deflections were recorded by taking photos with a digital camera from the rotating brush at speeds of 0–1200 rpm. Additional tests with only the duct frame were conducted to check certain assumptions used in the free-body diagrams. These tests are explained in Chapter 5.3. Preliminary laboratory tests with a rotating brush were performed earlier in the Laboratory for Mechanics of Materials at Helsinki University of Technology [12]. The experience obtained from these tests was useful for setting up the present laboratory arrangement.

Figure 5.2 presents some further details of the dimensions of the instrumentation in the laboratory test.

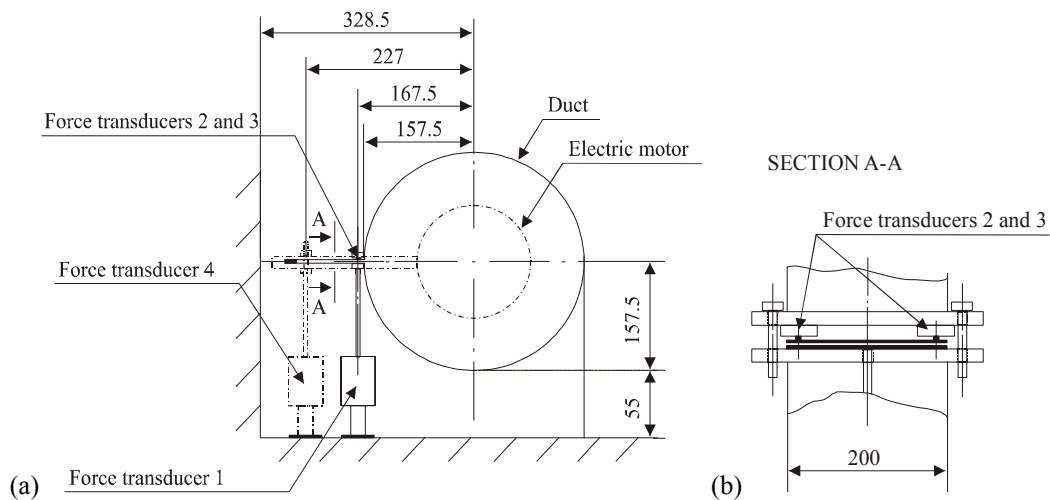


Fig. 5.2. (a) Instrumentation of the laboratory test. (b) Detail of the transducers installed in the seam of the duct frame on the left-hand side. Length units are given in mm.

Two free-body diagrams of the duct frame used in the analysis of the measurement results are shown in Figure 5.3. The frame is viewed in a similar way as is done in Figure 5.2, that is from the opposite direction of the motor. The rotation direction of

the motor and the brush shown in the diagrams is referred to here and in the following as being in the counterclockwise direction.

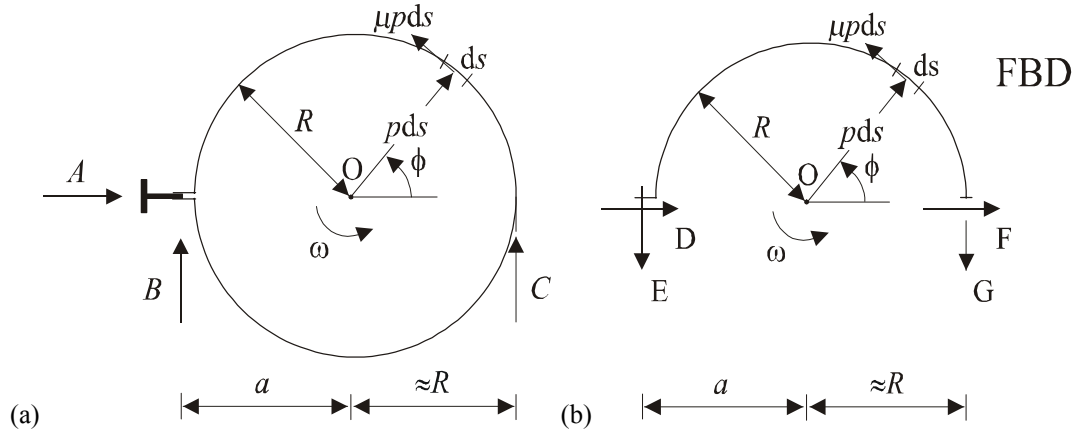


Fig. 5.3. (a) Free-body diagram of the frame. (b) Free-body diagram of the upper part of the frame.

5.2 Solution details

We represent the contact forces by "equivalent" uniform line loadings p and μp per unit length ($[p] = \text{N/m}$), where

$$p = \frac{nN}{2\pi R} \quad (5.4)$$

and where n is the total number of bristles. Thus, the differential force components acting on an arc length

$$ds = R d\phi \quad (5.5)$$

are $p ds$ and $\mu p ds$. We consider first the free-body diagram in Figure 5.3 (a). Force B represents the force read from transducer 1 and is positive if acting on the frame in the direction shown. Forces A and C are from the supporting plates of the frame. It is assumed that the plates are very flexible compared to the rigidity of the frame and thus the possible shearing forces and bending moments in the plates are neglected in the free-body-diagram. The equilibrium equations from the free-body diagram are

$$\rightarrow \quad A = 0, \quad (5.6)$$

$$\uparrow \quad B + C = 0, \quad (5.7)$$

$$0 \curvearrowright -B \cdot a + C \cdot R + T_\mu = 0, \quad (5.8)$$

where

$$T_\mu = \int_0^{2\pi} \mu p R d\phi \cdot R = \int_0^{2\pi} \mu \frac{nN}{2\pi R} R^2 d\phi = \mu n N R. \quad (5.9)$$

It can be seen for symmetry reasons without actual calculations that the contributions from pds and μpds cancel in (5.6) and (5.7). The solution of (5.6), (5.7) and (5.18) is

$$A = 0, \quad (5.10)$$

$$B = \frac{\mu n N R}{a + R} = \frac{\mu n N}{\frac{a}{R} + 1}, \quad (5.11)$$

$$C = -B. \quad (5.12)$$

Thus, we obtain

$$N = \frac{\left(\frac{a}{R} + 1\right) B}{n \mu}. \quad (5.13)$$

This could be used to evaluate the tip normal force N if μ were known in advance. However, this is usually not the case.

Without needing to draw a new free-body-diagram we can see that the torque required to resist the contact friction from the motor is also

$$T_\mu = T - (T_{ad} + T_{bf}) = \mu n N R. \quad (5.14)$$

The last form - also appearing in (5.9) - gives a formula for evaluating T_μ from the simulation. Alternatively, using the measured value for B and formulas (5.9) and (5.13):

$$T_\mu = B(a + R). \quad (5.15)$$

We next consider the free-body-diagram in Figure 5.3 (b) used for including the opening force E given by the sum of the forces in transducers 2 and 3 and assumed to be positive when acting on the frame in the direction shown. One of the assumptions

used is that the bending moments in the frame at the horizontal cuts are small and are neglected here. The equilibrium equations are

$$\rightarrow D + F + F_x = 0, \quad (5.16)$$

$$\uparrow -E - G + F_y = 0, \quad (5.17)$$

$$0 \cdot \curvearrowright E \cdot a - G \cdot R + \frac{1}{2}T_\mu = 0, \quad (5.18)$$

where

$$F_x = -\int_0^\pi \mu p R d\phi \cdot \sin \phi = -\int_0^\pi \mu \frac{nN}{2\pi R} R \sin \phi d\phi = -\frac{\mu nN}{\pi}, \quad (5.19)$$

$$F_y = \int_0^\pi p R d\phi \cdot \sin \phi = \int_0^\pi \frac{nN}{2\pi R} R \sin \phi d\phi = \frac{nN}{\pi}, \quad (5.20)$$

$$\frac{1}{2}T_\mu = \frac{1}{2}\mu nNR. \quad (5.21)$$

Some symmetries have been made use of when evaluating (5.19) and (5.20) so that certain terms are cancelled out. We can only determine the sum $D + F$, however, we are not interested in this and we will not make any use of (5.16). Eqs. (5.17) and (5.18) are, after some modifications, using matrix notation for clarity,

$$\begin{bmatrix} 1 & 1 \\ a & -R \end{bmatrix} \begin{bmatrix} E \\ G \end{bmatrix} = nN \begin{bmatrix} 1/\pi \\ -\mu R/2 \end{bmatrix}. \quad (5.22)$$

The solution, for example, using Cramer's rule is

$$E = \frac{D_1}{D} = \frac{nNR \left(-\frac{1}{\pi} + \frac{\mu}{2} \right)}{-(a+R)} = \frac{nN \left(\frac{1}{\pi} - \frac{\mu}{2} \right)}{\frac{a}{R} + 1}, \quad (5.23)$$

$$G = \frac{D_2}{D} = \frac{-nNR \left(\frac{a}{\pi R} + \frac{\mu}{2} \right)}{-(a+R)} = \frac{nN \left(\frac{1}{\pi} + \frac{\mu}{2} \right)}{\frac{a}{R} + 1}. \quad (5.24)$$

Together with (5.11) and (5.23) we have the set

$$\frac{n\mu N}{\frac{a}{R} + 1} = B, \quad (5.25)$$

$$\frac{nN\left(\frac{1}{\pi} - \frac{\mu}{2}\right)}{\frac{a}{R} + 1} = E. \quad (5.26)$$

The equations are linear in N and μN so we write them first as

$$\mu N = \left(\frac{a}{R} + 1\right) \frac{B}{n}, \quad (5.27)$$

$$\frac{N}{\pi} - \frac{\mu N}{2} = \left(\frac{a}{R} + 1\right) \frac{E}{n}. \quad (5.28)$$

Replacing μN in Eq. (5.28) with (5.27) and after some manipulation

$$N = \left(\frac{a}{R} + 1\right) \left(\frac{B}{2} + E\right) \frac{\pi}{n}, \quad (5.29)$$

$$\mu = \frac{B}{\left(\frac{B}{2} + E\right)\pi} = \frac{1}{\left(\frac{1}{2} + \frac{E}{B}\right)\pi}. \quad (5.30)$$

Thus we now have, in theory, formulas for obtaining both the bristle contact normal force and the coefficient of friction using the measured data. The calculations performed above are based on assuming the rotation direction of the brush to be counterclockwise. If the rotation direction is changed, the friction force elements $\mu p ds$ act in the opposite directions in the new free-body-diagrams corresponding to Figures 5.3 (a) and 5.3 (b). The end results are that (5.11) changes to the opposite value (we denote the quantities now with a dash)

$$B' = -\frac{n\mu' N'}{\frac{a}{R} + 1} \quad (5.31)$$

and (5.22) changes to

$$\begin{bmatrix} 1 & 1 \\ a & -R \end{bmatrix} \begin{bmatrix} E' \\ G' \end{bmatrix} = nN' \begin{bmatrix} 1/\pi \\ \mu' R/2 \end{bmatrix}. \quad (5.32)$$

The new opening force becomes

$$E' = \frac{nN' \left(\frac{1}{\pi} + \frac{\mu'}{2} \right)}{\frac{a}{R} + 1}. \quad (5.33)$$

Thus the presence of friction should be seen as a dependence of the opening force on the rotation direction. The counterparts of Eqs. (5.27) and (5.28) become

$$-\mu' N' = \left(\frac{a}{R} + 1 \right) \frac{B'}{n}, \quad (5.34)$$

$$\frac{N'}{\pi} + \frac{\mu' N'}{2} = \left(\frac{a}{R} + 1 \right) \frac{E'}{n}. \quad (5.35)$$

We obtain

$$N' = \left(\frac{a}{R} + 1 \right) \left(\frac{B'}{2} + E' \right) \frac{\pi}{n}, \quad (5.36)$$

$$\mu' = \frac{-B'}{\left(\frac{B'}{2} + E' \right) \pi} = - \frac{1}{\left(\frac{1}{2} + \frac{E'}{B'} \right) \pi}. \quad (5.37)$$

According to (5.23) E changes its sign from positive to negative at

$$\mu = \frac{2}{\pi} \approx 0.64. \quad (5.38)$$

However, E' according to (5.33) is positive. The results from Eqs. (5.29) and (5.30) as well as Eqs. (5.36) and (5.37) are described in Chapter 6.

5.3 Additional test

To gain some confidence in the assumptions used in connection with the free-body diagrams, two simple additional tests were performed on the frame without a brush. In case 1 a small body weighing $W=4.91$ N was set at the top of the duct frame and in case 2 at the bottom of the frame. The corresponding free-body diagrams are shown in Figures 5.4 (a) and (b) and Figures 5.4 (c) and (d), respectively.

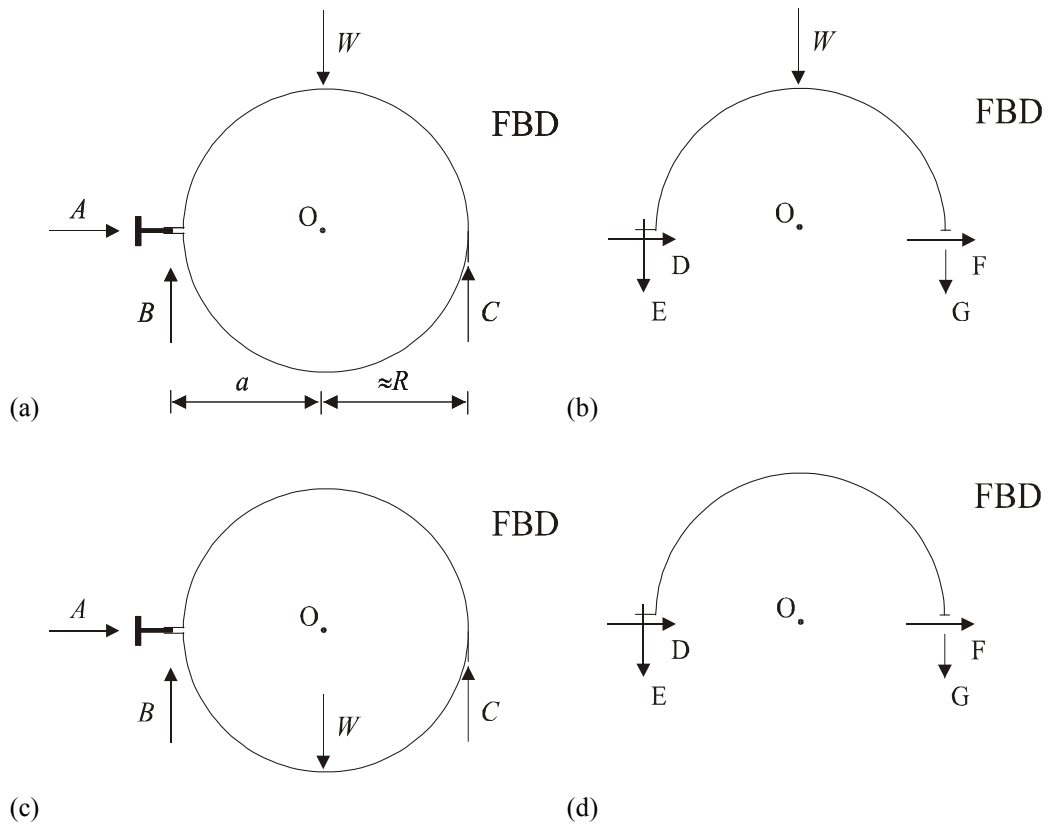


Fig. 5.4. (a) Free-body diagram of the frame. (b) Free-body diagram of the upper part of the frame (case 1). (c) Free-body diagram of the frame. (d) Free-body diagram of the upper part of the frame (case 2).

In case 1 we obtain the equilibrium equations (Figure 5.4 (a) and (b))

$$\rightarrow A = 0, \quad (5.39)$$

$$\uparrow B + C - W = 0, \quad (5.40)$$

$$0 \cdot \curvearrowright -B \cdot a + C \cdot R = 0, \quad (5.41)$$

and

$$\rightarrow D + F = 0, \quad (5.42)$$

$$\uparrow -E - G - W = 0, \quad (5.43)$$

$$0 \cdot \curvearrowright E \cdot a - G \cdot R = 0. \quad (5.44)$$

These give

$$B = \frac{W}{1 + \frac{a}{R}}, \quad (5.45)$$

$$E = -\frac{W}{1 + \frac{a}{R}}. \quad (5.46)$$

In case 2, Eqs. (5.39)–(5.41) are still valid but W disappears from Eq. (5.43). Thus, the solution is

$$B = \frac{W}{1 + \frac{a}{R}}, \quad (5.47)$$

$$E = 0. \quad (5.48)$$

Table 5.1 presents a comparison of the calculated and measured results with $a=0.1675$ m and $R=0.1575$ m.

Table 5.1. Results of the check on the free-body assumptions

Force	Case 1			Case 2		
	Calculated (N)	Measured (N)	Diff. (%)	Calculated (N)	Measured (N)	Diff. (%)
B	2.377 ^a	2.256	5.1	2.377 ^c	2.531	–6.5
E	–2.377 ^b	–2.590	–9.0	0 ^d	0.02943	–

^a Eq. (5.45), ^b Eq. (5.46), ^c Eq. (5.47), ^d Eq. (5.48)

The measured results in this additional test may be viewed as being rather close to the theoretical values obtained using the same assumptions employed above in the cases that included the brush. Thus, these results give certain confidence in the validity of the assumptions and also a rough idea of the errors included. Further, the weight ($W=4.91$ N) corresponds roughly to the mean value of measured B (~ 0 – 10 N) and E (-1 – 8 N) in Figure 6.7.

6 RESULTS

6.1 Simulation details

In all the calculations described below the bristle cross section was taken to be circular and the length $L = 0.175$ m, diameter $d = 1 \times 10^{-3}$ m, cross-sectional moment of inertia $I = \pi d^4 / 64 = 4.909 \times 10^{-14}$ m⁴, density $\rho_b = 1140$ kg/m³, friction coefficient $\mu = \pi_3 = 0.7$, kinematic viscosity of air $\nu_a = 1.528 \times 10^{-5}$ m²/s, bristle length duct radius ratio $\zeta = \pi_2 = L/R = 1.111$ ($R = 0.1575$ m) and Young's modulus $E = 2.8$ GPa, where the latter corresponds roughly to the data for nylon [13]. The friction coefficient value was estimated from the results of the present laboratory tests (Figure 6.10). The effect of air drag was studied by using the reduced air speed coefficient value $c = 0$ (no air drag) and $c = 1$ ("full" air drag). The simulations were performed for a brush where the number of bristles was $n = 1000$.

6.2 Rotating bristle calculations

6.2.1 Deflection of rotating bristle

Figure 6.1 shows the deflection of a bristle with the rotation speed of 0 rpm, 500 rpm, 1000 rpm and 2000 rpm in a duct.

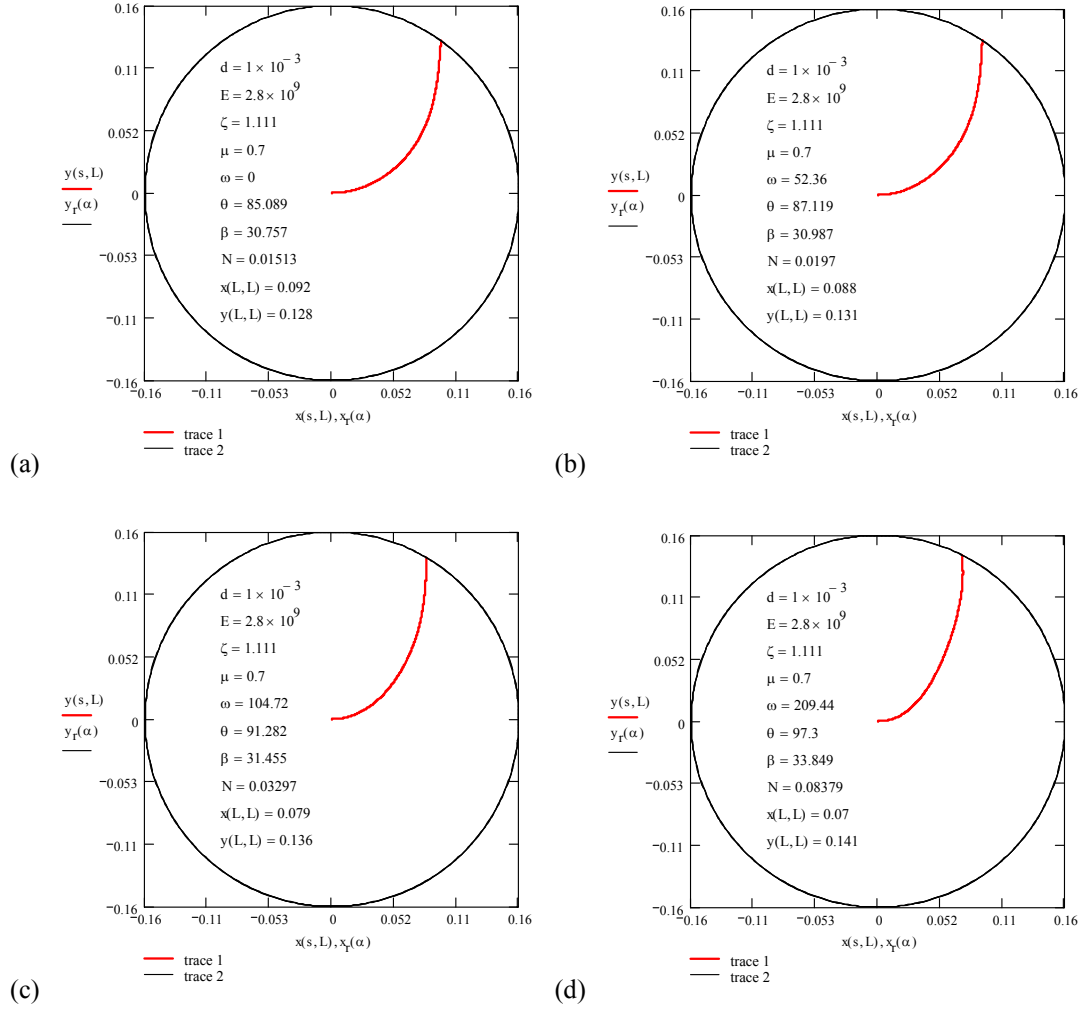


Fig. 6.1. Deflected form of the bristle [m] (a) bristle rotation speed $n=0$ rpm, (b) $n=500$ rpm, (c) $n=1000$ rpm and (d) $n=2000$ rpm in a duct. The units of the quantities in the figures are $[d]=\text{m}$, $[E]=\text{Pa}$, $[\zeta]=-$, $[\mu]=-$, $[\omega]=\text{rad/s}$, $[\theta]=^\circ$, $[\beta]=^\circ$, $[N]=\text{N}$, $[x]=\text{m}$, $[y]=\text{m}$.

The deflected shape of the bristle changes with the rotation speed of the bristle. In a stationary situation the bristle is deformed rather symmetrically with respect to its ends. As the rotation speed of the bristle increases the deformation seems to concentrate near the rotation centre. Reference [2, Figure 4.2] presents the results of the deflected shape of the bristle calculated by using the friction coefficient value $\mu = 0.5$.

6.2.2 Dependence on the rotation speed of the bristle

Figure 6.2 presents the magnitude of the simulated normal force N_s and the contact angle β_s as a function of the rotation speed of a bristle in the duct.

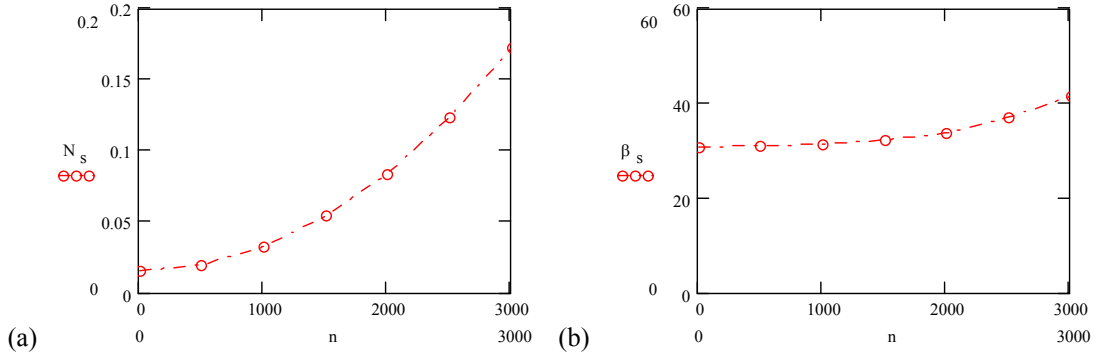


Fig. 6.2. (a) The magnitude of simulated normal force N_s [N] and (b) contact angle β_s [°] as functions of the rotation speed n [rpm] in the duct.

Initially, the magnitude of the normal force N_s increases roughly quadratically in the interval of 0–3000 rpm, which corresponds to the value $\pi_1 = 0 - 550$. However, when n is higher than the unrealistic values of 8000 rpm (this corresponds approximately to the value $\pi_1 = 4000$), the magnitude of the normal force was found to only increase slowly. The contact angle β_s increases most strongly roughly in the same rotation speed range as the magnitude of the normal force. The contact angle has its maximum value approximately at the rotation speed of 10000 rpm. However, the comparison between the results of the model and the experimental data limits at speeds of 200–1200 rpm (Figure 6.7), which corresponds roughly to the practical rotating speed in mechanical brushing.

6.2.3 Dependence on air drag

Figure 6.3 shows the deflection of a bristle without ($c = 0$) and with air drag ($c = 1$) as functions of the rotation speed of a bristle in the duct.

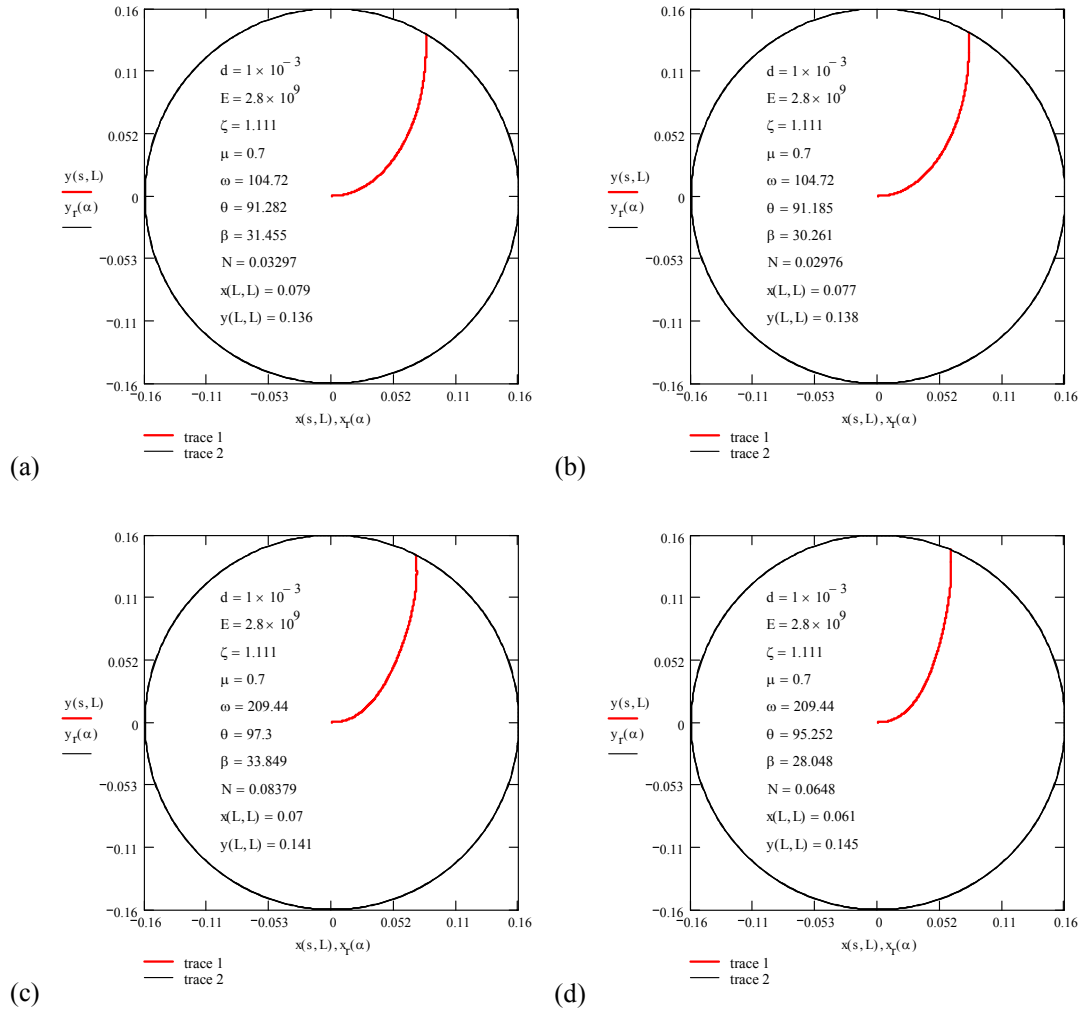


Fig. 6.3. Deflected form of the bristle [m] (a) The bristle rotates at the speed of 1000 rpm without air drag and (b) with air drag. (c) The bristle rotates at the speed of 2000 rpm without air drag and (d) with air drag in a duct.

Air drag only slightly affects the deflection of the single bristle at rotation speeds of 1000 rpm and 2000 rpm. As is to be expected, the deformation of the bristle due to air drag is more concentrated near the rotation centre as it can be observed at the rotation speed of 2000 rpm.

Figure 6.4 presents the magnitude of simulated normal force N_s and the contact angle β_s without and with air drag as functions of the rotation speed of a bristle in the duct.

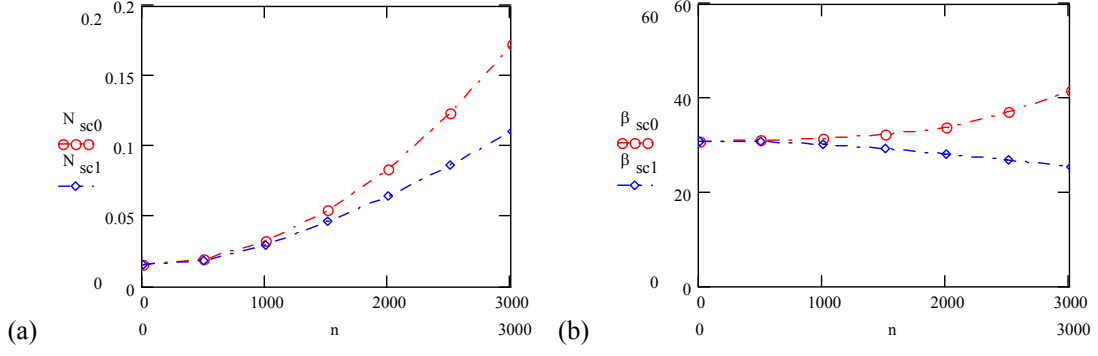


Fig. 6.4. (a) The magnitude of simulated normal force N_s [N] and (b) contact angle β_s [°] without and with air drag as functions of the rotation speed n [rpm] in the duct.

Air drag decreases both the magnitude of normal force and the contact angle. Due to air drag, the magnitude of the normal force decreases 10% and 23% at the rotation speeds of 1000 rpm and 2000 rpm, respectively. Without air drag the contact angle increases in the range of 0–3000 rpm. As expected, the contact angle decreases due to air drag when rotation speed increases.

The bending moment in a bristle at the origin evaluated from the deformed shape is $-EI d\theta(0)/ds$. Taking into account the sign conventions used, the torque from the brush (number of the bristles n) evaluated from this is thus [3]

$$T_b = nEI \frac{d\tilde{\theta}}{ds}(0). \quad (6.1)$$

The torque from a brush due to air drag is evaluated from [3]

$$T_{ad} = n \int_0^L q(s')r(s')\cos\gamma(s')ds'. \quad (6.2)$$

The integral was calculated by approximating the integrand by Lagrangian interpolation with four interpolation points $s_1 = 0$, $s_2 = L/3$, $s_3 = 2L/3$ and $s_4 = L$.

Figure 6.5 presents the magnitude of the simulated torques T_{bs} (Eq. (6.1)) and the torque $T_{\mu ads}$ from a brush due to friction (5.14) and air drag (Eq. (6.2)) from

$$T_{\mu ads} = \mu nNR + n \int_0^L q(s')r(s')\cos\gamma(s')ds' \quad (6.3)$$

as functions of the rotation speed of the brush in the duct.

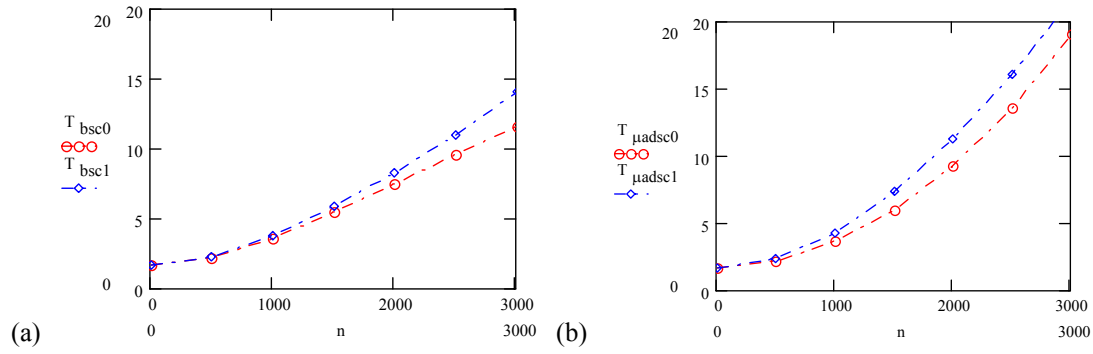


Fig. 6.5. (a) The magnitude of simulated torque T_{bs} [Nm] without and with air drag as functions of the rotation speed n [rpm]. (b) The magnitude of simulated torque $T_{\mu ads}$ [Nm] without and with air drag as functions of the rotation speed n [rpm].

The torques T_{bs} and $T_{\mu ads}$ increase roughly quadratically in the interval of 0–3000 rpm and are roughly the same magnitude (with $c = 1$) when the rotation speed is below 1000 rpm (difference below 13%). After this, the difference increases quickly as a function of the rotation speed of the bristle. Without discretization errors the torques T_{bs} and $T_{\mu ads}$ should be in theory equal here. The values of $T_{\mu ads}$ are probably much more reliable as they are integrated quantities. T_{bs} gives a local result, which is sensitive to small changes in the value of the parameter c_1 . Reference [3] presents in more detail the dependence on air drag.

6.3 Results of laboratory test

6.3.1 Deflection of bristle

Figure 6.6 shows the deflection of the bristle pair and the brush with the rotation speeds of 0 rpm, 500 rpm and 1000 rpm (clockwise direction) in the duct.

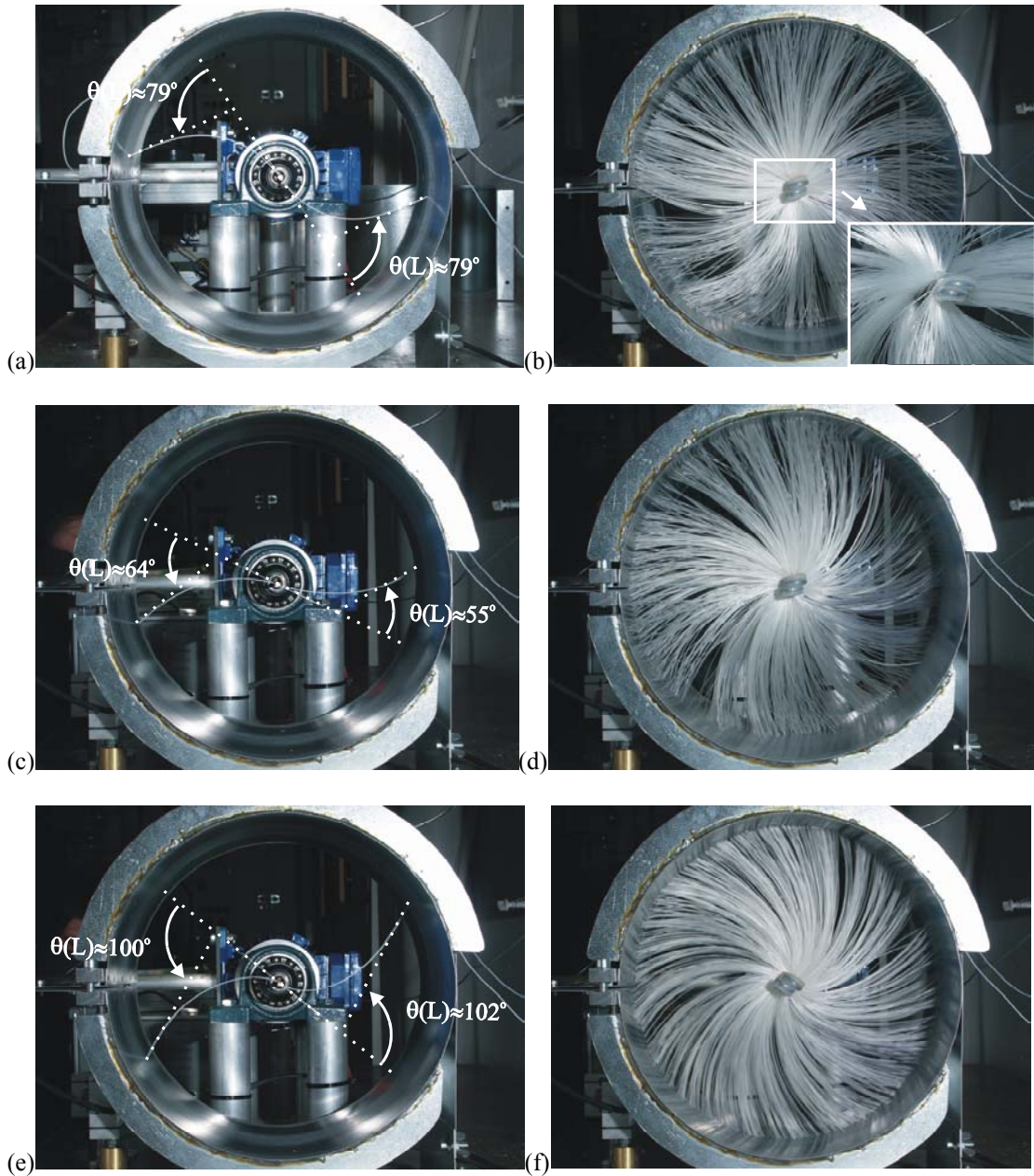


Fig. 6.6. Deflected form of the bristle (a) bristle rotation speed $n=0$ rpm, (c) $n=500$ rpm and (e) $n=1000$ rpm in the duct with contact. Deflected form of the brush (b) brush rotation speed $n=0$ rpm, (d) $n=500$ rpm and (f) $n=1000$ rpm in the duct with contact.

The deflection of the bristle pair is quite similar to that obtained by the simulation with $n = 0$ rpm and $n = 1000$ rpm. At a rotation speed of $n = 500$ rpm the bristle pair was found not to remain in the plane assumed in the simulation and therefore the deflection of the bristle pair seen in the photograph is low compared to that obtained by the simulation. The deflections of bristles of the brush are difficult to estimate accurately

because the bristles were connected asymmetrically on a spiral frame made of metal wire (Figure 6.6 (b)).

Figures 6.7 (a) and (b) give the measurement results for force P (transducer 4), Figures (c) and (d) for force B (transducer 1) and Figures (e) and (f) for force E (transducers 2 and 3) as functions of the rotation speed, when the brush is in contact with the duct.

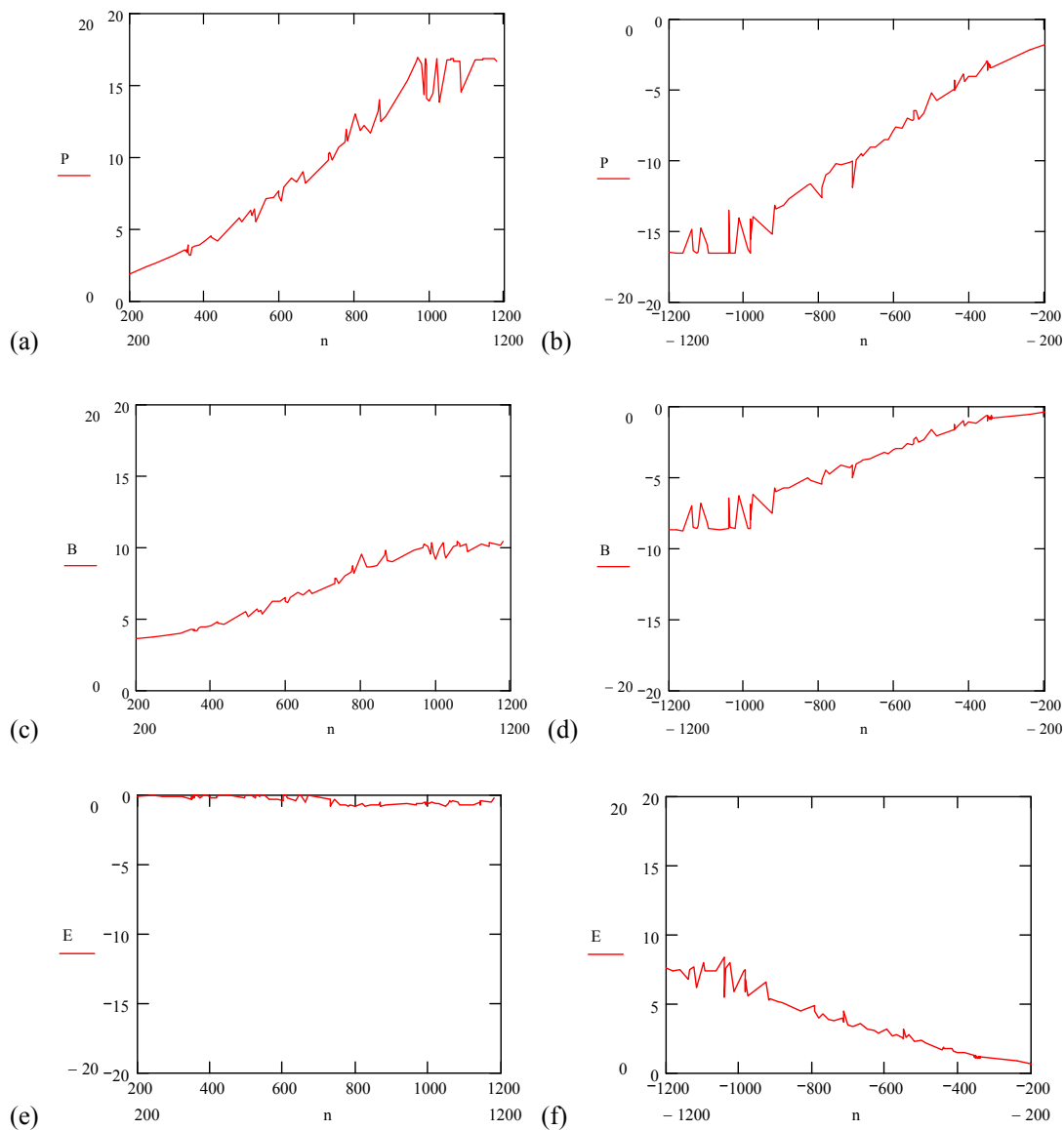


Fig. 6.7. The magnitude of forces P [N], B [N] and E [N] as functions of the rotation speed n [rpm].

The behaviour of force E with respect to rotation direction is qualitatively in accordance with the theory. From Eq. (5.23), the friction coefficient has to be higher

than 0.64 if E becomes negative when the brush is rotated in the counterclockwise direction (Figure 6.8 (e)). For low magnitudes of n , there is quite a large difference in the magnitudes of force B with respect to the rotation direction; in theory the magnitudes should be equal.

With regard to the figures presenting experimental results in general we may note the following. The counterclockwise rotation direction is again considered positive with respect to the rotation speed n . No values are given when the magnitude of n is under 200 rpm as the measured data may be considered rather unreliable with the corresponding small forces. The oscillations in the data are mainly due to the unavoidable vibration generated in the test system. For most quantities presented here the magnitudes should in theory be equal for a given magnitude of n in the counterclockwise and clockwise directions. In practice, the brush has some directional bias due to its construction (see Figure 6.6 (b)). Further, the bristle tips wear out on contact and may also show directional asymmetry, etc.

6.3.2 Magnitude of normal force

Figure 6.8 presents the bristle tip normal force N evaluated from measured data by Eqs. (5.29) and (5.36) as well as the simulated results N_s without and with air drag as functions of the rotation speed.

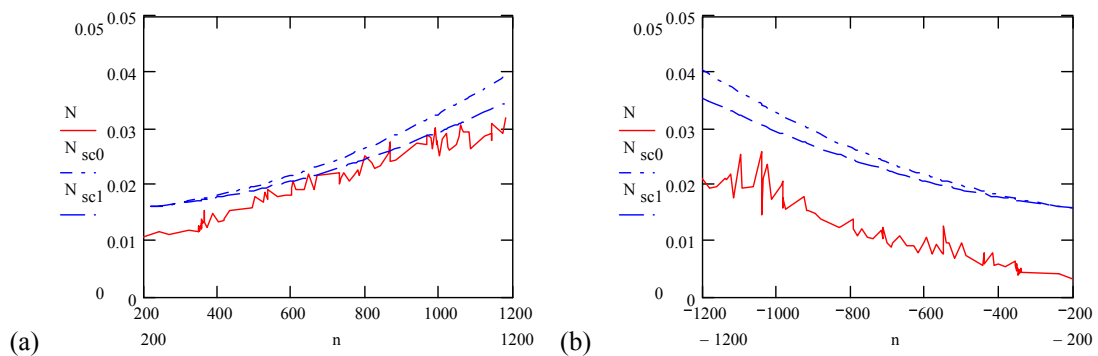


Fig. 6.8. The measured N [N] and simulated normal force N_s [N] without and with air drag as functions of the rotation speed n [rpm].

The increment of the experimental and simulated values are roughly of the same order with $c = 0$ (no air drag) at rotation speeds of 500–1000 rpm. There is quite a

difference in the experimental results with respect to the rotation direction and it is difficult to judge which results are more reliable. It may be noticed that already the seeming well-controlled cases with results in Table 5.1 showed errors between the calculated and the measured values. Additionally, the possible deviations of the bristles from the plane (see Figure 5.1) assumed in the simulation may explain the somewhat lower values obtained in the experiment.

6.3.3 Magnitude of torque

Figures 6.9 (a) and (b) present torque T_μ due to friction from the brush obtained from the measuring results (Eq. (5.15)) and from the simulation, $T_{\mu s}$ (Eq. (5.14)) evaluated as functions of rotation speed.

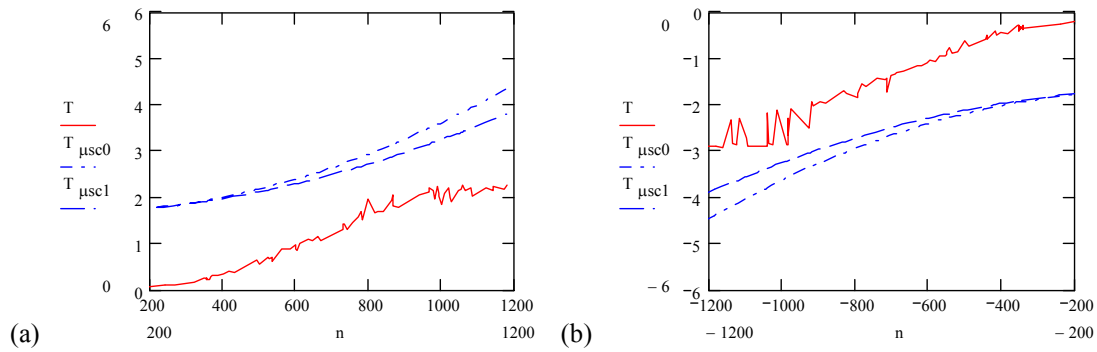


Fig. 6.9. The measured torque T_μ [Nm] and simulated torque $T_{\mu s}$ [Nm] without and with air drag (included through N) as functions of the rotation speed n [rpm].

The magnitude of the torque T_μ from measured data and simulated values $T_{\mu s}$ differ. However, the "slopes" of measured and simulated curves with $c = 0$ seem to be rather close to each other. The possible explanations for the difference between the calculated and the measured values are the same as in the previous Chapter (6.3.2).

6.3.4 Friction coefficient

Figure 6.10 presents friction coefficient μ evaluated by Eqs. (5.30) and (5.37) as functions of the rotation speed.

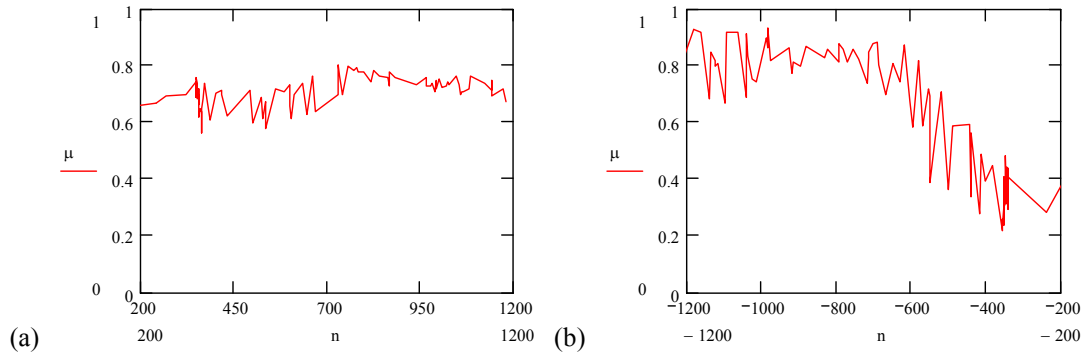


Fig. 6.10. The friction coefficient μ [-] as function of the rotation speed n [rpm].

The reason for low values for μ obtained for low rotation speeds in the clockwise direction may be arise from the inconsistent behaviour of force B , which was discussed in connection with Figure 6.7. In any case, the average values (roughly 0.7 and 0.65) are clearly higher than those (roughly 0.5) obtained for nylon in [14] with a different test arrangement. Because of the high friction coefficient, the tips of the bristle pair were worn rapidly when the rotation speed was higher than 2000 rpm. Based on the results in Figure 6.10, we have used the value $\mu = 0.7$ in the simulations.

Furthermore, the maximum rotation speed achieved was approximately 1200 rpm with an electrical motor that has a power of 0.25 kW [12] and also with a motor that has a power of 0.55 kW. When friction between the bristle tip and the duct surface was decreased artificially with a mixture of water and a detergent, the rotation speed of the brush achieved a value of 2500 rpm.

6.4 Summary of the results

Table 6.1 summarizes the dependence of the normal force N and the contact angle β as a function of the dimensionless numbers π_1 , π_2 and π_3 . The values of $\pi_1 = \rho AL^4 \omega^2 / EI = 15.4$, $\pi_2 = L/R = 1.1$ and $\pi_3 = \mu = 0.5$ were used for the rest of the quantities, except for the parameters in question which were varied to observe their effect on the results. The percentage changes are referred to the values obtained by the lower values of the three parameters. Reference [2] presents the dependence of the normal force and the contact angle on n , R , d , E , L/R and μ .

Table 6.1. Dependence of normal force and contact angle on various parameters

Dimensionless number (range)	Normal force N		Contact angle β	
	influence	difference [%]	influence	difference [%]
$\pi_1 = \rho AL^4 \omega^2 / EI$ ($\pi_1 = 0-500$)	+++	916	+	40
$\pi_2 = L/R$ ($\pi_2 = 1.05-1.3$)	+	45	+++	145
$\pi_3 = \mu$ ($\pi_3 = 0.1-0.9$)	--	-67	-	-21

-/+ = negative/positive dependence ($5\% < \text{difference} \leq 50\%$)

--/+ += strong negative/positive dependence ($50\% < \text{difference} \leq 100\%$)

-- -/+ += very strong negative/positive dependence ($\text{difference} > 100\%$)

Table 6.2 summarizes the results for the normal force N and torque T at rotation speeds of 500 rpm and 1000 rpm obtained from the simulation ($T_{\mu s}$ from Eq. (5.14)) and the experimental test (N from Eqs. (5.29) and (5.36) and T_{μ} from Eq. (5.15)), respectively.

Table 6.2. Magnitude of simulated and measured normal force and torque

Simulated and experimental results	Normal force N [N]		Torque T [Nm]	
	($c = 0$)	($c = 1$)	($c = 0$)	($c = 1$)
Simulation				
Rotation speed $n = 500$ rpm	0.0197	0.0191	2.184	2.119
Rotation speed $n = 1000$ rpm	0.0328	0.0295	3.623	3.248
Experimental test				
Counterclockwise direction				
Rotation speed $n = 500$ rpm ^a	0.0168		0.669	
Rotation speed $n = 1000$ rpm ^b	0.0280		2.095	
Clockwise direction				
Rotation speed $n = 500$ rpm ^a	0.0082		-0.758	
Rotation speed $n = 1000$ rpm ^b	0.0190		-2.521	

^a mean value of $n = 400 - 600$ rpm

^b mean value of $n = 900 - 1100$ rpm

7 DISCUSSION

The authors assumed that the normal force N and the contact angle β were the most important parameters associated with a bristle in removing dust on the duct surface. As is mentioned in Chapter 1, theoretical and experimental work is needed to clarify the roles of N and β in the cleaning process. Figure 7.1 presents a possible schematic experimental arrangement for a laboratory test to determine the cleaning efficiency of a bristle with a given N and β [15].

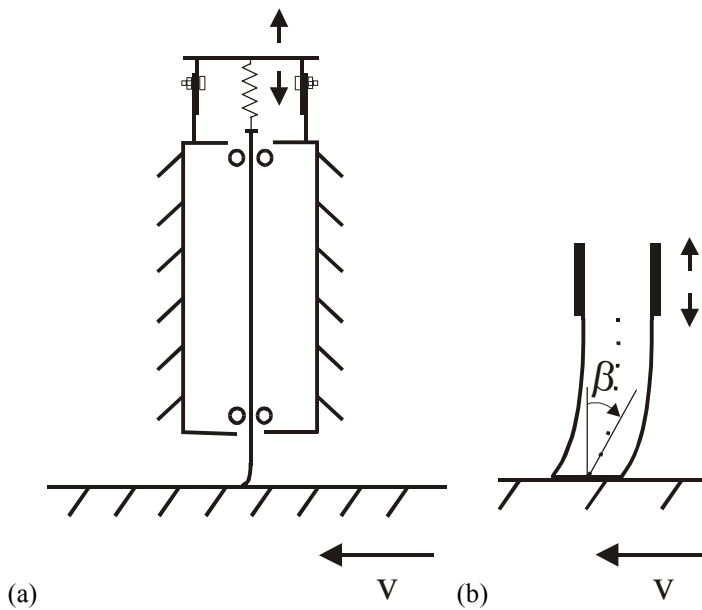


Fig. 7.1. (a) Experimental arrangement to determine the cleaning efficiency of a bristle. (b) Bristle tip.

The experimental arrangement consists of a long spring with an adjustable upper end position to fix the contact force N , a bristle holder tube suspended to the spring, bearings with low friction to guide the movement of the bristle holder up and down, and a moving surface. In the test, the bristle tip contacts to the surface which moves at the speed of v . The bristle tip contact angle is adjusted by changing the free length of the bristle between the end of the holder and the surface. The cleaning efficiency is evaluated following in the bristle tip track on the surface. To make sure that the test can be repeated, the surface should be artificially contaminated.

It is obvious that without a centralizing device the rotation centre of the brush cannot situate exactly at the centre of the duct. Some eccentricity is needed for the contact forces of the brush to produce an upwards directed resultant to give equilibrium with gravity. If the rotation centre of the brush remains roughly stationary, each brush obtains a periodic motion in the rotating coordinate system. To study this with reasonable accuracy would demand a much greater effort than has been employed in this article. It should be further mentioned that taking the gravity of an individual bristle into account, even in the case of no eccentricity, leads in fact to a periodic response as the direction of the gravity in the rotating coordinate system depends on the orientation of the coordinate system.

The approximation used in the simulation of the rotating bristle problem is rather crude. Higher order Lagrangian interpolation functions could be used. However, it is well-known that these start to behave badly at the ends of the interval, therefore it appears to be unwise to go higher than $n=4$ [16]. An alternative to the use of Lagrangian interpolation is just to employ, say, Simpson's integration rule in a double fashion. Then the number of integration points can be selected to be as large as is required without any danger of ill-behaviour. This alternative is described in [11]. It was found that with practical data the results obtained by using the present approach and by the approach using Simpson's rule were rather close. Here we have tried to keep the formulation as close as possible to an analytical approach and have relied on the Lagrange interpolation method.

8 CONCLUSION

An improved simple model was used to evaluate the magnitude of the normal force N and the contact angle β of the rotating bristle tip on the duct surface. The dimensionless formulation was employed to simplify the dependencies between the various parameters and to make the brush cleaning design process as systematic as possible. The magnitude of the dimensionless normal force \bar{N} increases roughly linearly with the dimensionless number π_1 at a practical rotation speed. With higher dimensionless number values of π_2 the bristle "has to bend more to fit in the duct" and the contact angle increases. Increasing the dimensionless number π_3 decreases the dimensionless normal force. The experimental results obtained in general give some confidence in the validity of the proposed simulation model to the extent that it can be used in analysing and comparing different brush designs. In conclusion, the developed simple simulation model combined with such programs as Mathcad software seems to be a useful tool in cleaning brush design work.

ACKNOWLEDGEMENTS

This study was carried out as a part of the Lifa Duct Cleaning Concept funded by Oy Lifa Air Ltd and the National Technology Agency, Finnish industry and participating research organisations. The authors would like to thank in particular following people; Iikka Järvenpää (laboratory manager) for his valuable comments in the laboratory test, Markku Sivukari (laboratory manager) and Petteri Kivivuori (mechanic) for arrangements for the laboratory test, Petteri Martonen for his preliminary test with a rotating brush, Marko Björkroth and Jarkko Narvanne for their help in taking photos from the laboratory tests, Professor Reijo Lappalainen for the laboratory test for determining friction between a bristle and a steel plate, and Leif Eriksson (laboratory manager) for the laboratory test for determining Young's modulus for the bristles.

REFERENCES

- [1] Holopainen R, Asikainen V, Tuomainen M, Björkroth M, Pasanen P, Seppänen, O. Effectiveness of Duct Cleaning Methods on Dusty and Oily Duct Surfaces. Accepted for publication by the International Journal of Indoor Environment and Health on 15th November, 2001.
- [2] Holopainen R, Salonen E-M. A simple model for analysing bristle contact force and contact angle in rotating brush duct cleaning. Helsinki University of Technology. Department of Mechanical Engineering. Laboratory of Heating, Ventilating and Air Conditioning. Report B72. 39 p. 2002.
- [3] Holopainen R, Salonen E-M. Rotating brush behaviour in duct cleaning. Helsinki University of Technology. Submitted for publication to the Experimental Mechanics on 17th April, 2003.
- [4] Timoshenko SP, Gere JM. Theory of Elastic Stability. McGraw-Hill Book Company 1961.
- [5] Schlichting H. Boundary-Layer Theory. McGraw-Hill Book Company 1979.
- [6] Blevins R. Flow-Induced Vibration. Van Nostrand Reinhold International Company Limited 1990.
- [7] Crandall SH. Engineering Analysis: A Survey of Numerical Procedures. McGraw-Hill Book Company 1956.
- [8] <http://www.mathcad.com/> (4th April, 2003).
- [9] <http://www.mathcad.com/library/> (4th April, 2003).
- [10] Burden RL, Faires JD. Numerical Analysis. PWS Publishing Company 1993.
- [11] Holopainen R, Salonen E-M. Large deformation analysis of a rotating bristle in brush duct cleaning. Accepted for publication for the 15th International conference on computer methods in mechanics (CMM-2003). 2003.
- [12] Martonen P. Puhdistusharjan ilmanvaihtokanavaan synnyttämien voimien kokeellinen määrittäminen. (Experimental determination of the forces from a rotating brush in a ventilation duct). Individual Assignments in Strength of Materials. Laboratory for Mechanics of Materials. Helsinki University of Technology. 2002. In Finnish.
- [13] Viljamaa A, Eriksson L. Polyamidin E-modulin mittaaminen. (Polyamide Young's modulus and its measuring in the laboratory). The Laboratory of

Processing and Heat Treatment of Materials. Helsinki University of Technology. 2003. In Finnish. Private communication.

- [14] Rautiainen S. Harjaksen ja teräspellin välinen kitka. (Friction between bristle and steel plate). Department of Applied Physics. University of Kuopio. 2002. In Finnish.
- [15] Lappalainen R. Experimental arrangement for a laboratory test to determine the cleaning efficiency of one bristle. Department of Applied Physics. University of Kuopio. 2003. Private communication.
- [16] Irons B, Ahmad S. Techniques of Finite Elements. Ellis Horwood Ltd 1980.

The boundary condition at the bristle tip (Eq. (3.24)):

$$g(C1, C2, C3, C4, C5, C6) := C1 + 2 \cdot C2 \cdot L + 3 \cdot C3 \cdot L^2 + 4 \cdot C4 \cdot L^3 + 5 \cdot C5 \cdot L^4 + 6 \cdot C6 \cdot L^5$$

The geometrical condition at the bristle tip with coordinates $x(L)$ and $y(L)$ on the duct surface (Eq. (3.25)):

$$h(C1, C2, C3, C4, C5, C6) := \left[\begin{array}{l} \frac{-1}{8} \cdot L \cdot \frac{(9 \cdot L^3 - 24 \cdot L \cdot L^2 + 22 \cdot L^2 \cdot L - 8 \cdot L^3)}{L^3} \cdot \cos(C1 \cdot 0 + C2 \cdot 0^2 + C3 \cdot 0^3 + C4 \cdot 0^4 + C5 \cdot 0^5 + C6 \cdot 0^6) \dots \\ + \frac{3}{8} \cdot L^2 \cdot \frac{(9 \cdot L^2 - 20 \cdot L \cdot L + 12 \cdot L^2)}{L^3} \cdot \cos \left[C1 \cdot \left(\frac{L}{3}\right) + C2 \cdot \left(\frac{L}{3}\right)^2 + C3 \cdot \left(\frac{L}{3}\right)^3 + C4 \cdot \left(\frac{L}{3}\right)^4 + C5 \cdot \left(\frac{L}{3}\right)^5 + C6 \cdot \left(\frac{L}{3}\right)^6 \right] \dots \\ + \frac{-3}{8} \cdot L^2 \cdot \frac{(9 \cdot L^2 - 16 \cdot L \cdot L + 6 \cdot L^2)}{L^3} \cdot \cos \left[C1 \cdot \left(\frac{2 \cdot L}{3}\right) + C2 \cdot \left(\frac{2 \cdot L}{3}\right)^2 + C3 \cdot \left(\frac{2 \cdot L}{3}\right)^3 + C4 \cdot \left(\frac{2 \cdot L}{3}\right)^4 + C5 \cdot \left(\frac{2 \cdot L}{3}\right)^5 + C6 \cdot \left(\frac{2 \cdot L}{3}\right)^6 \right] \dots \\ + \frac{1}{8} \cdot L^2 \cdot \frac{(9 \cdot L^2 - 12 \cdot L \cdot L + 4 \cdot L^2)}{L^3} \cdot \cos(C1 \cdot L + C2 \cdot L^2 + C3 \cdot L^3 + C4 \cdot L^4 + C5 \cdot L^5 + C6 \cdot L^6) \end{array} \right]^2 \\ + \left[\begin{array}{l} \frac{-1}{8} \cdot L \cdot \frac{(9 \cdot L^3 - 24 \cdot L \cdot L^2 + 22 \cdot L^2 \cdot L - 8 \cdot L^3)}{L^3} \cdot \sin(C1 \cdot 0 + C2 \cdot 0^2 + C3 \cdot 0^3 + C4 \cdot 0^4 + C5 \cdot 0^5 + C6 \cdot 0^6) \dots \\ + \frac{3}{8} \cdot L^2 \cdot \frac{(9 \cdot L^2 - 20 \cdot L \cdot L + 12 \cdot L^2)}{L^3} \cdot \sin \left[C1 \cdot \left(\frac{L}{3}\right) + C2 \cdot \left(\frac{L}{3}\right)^2 + C3 \cdot \left(\frac{L}{3}\right)^3 + C4 \cdot \left(\frac{L}{3}\right)^4 + C5 \cdot \left(\frac{L}{3}\right)^5 + C6 \cdot \left(\frac{L}{3}\right)^6 \right] \dots \\ + \frac{-3}{8} \cdot L^2 \cdot \frac{(9 \cdot L^2 - 16 \cdot L \cdot L + 6 \cdot L^2)}{L^3} \cdot \sin \left[C1 \cdot \left(\frac{2 \cdot L}{3}\right) + C2 \cdot \left(\frac{2 \cdot L}{3}\right)^2 + C3 \cdot \left(\frac{2 \cdot L}{3}\right)^3 + C4 \cdot \left(\frac{2 \cdot L}{3}\right)^4 + C5 \cdot \left(\frac{2 \cdot L}{3}\right)^5 + C6 \cdot \left(\frac{2 \cdot L}{3}\right)^6 \right] \dots \\ + \frac{1}{8} \cdot L^2 \cdot \frac{(9 \cdot L^2 - 12 \cdot L \cdot L + 4 \cdot L^2)}{L^3} \cdot \sin(C1 \cdot L + C2 \cdot L^2 + C3 \cdot L^3 + C4 \cdot L^4 + C5 \cdot L^5 + C6 \cdot L^6) \end{array} \right]^2$$

Discrete equations by collocation with four collocation points and by Lagrangian interpolation with seven subintervals within a Mathcad solve block:

Given

$$\text{Eq. (3.22), } s_1=0: \quad f(C1, C2, C3, C4, C5, C6, N, 0) = 0$$

$$\text{Eq. (3.22), } s_2=L/4: \quad f \left(C1, C2, C3, C4, C5, C6, N, \frac{L}{4} \right) = 0$$

$$\text{Eq. (3.22), } s_3=L/2: \quad f \left(C1, C2, C3, C4, C5, C6, N, \frac{L}{2} \right) = 0$$

$$\text{Eq. (3.22), } s_4=3L/4: \quad f \left(C1, C2, C3, C4, C5, C6, N, \frac{3 \cdot L}{4} \right) = 0$$

$$\text{Eq. (3.22), } s_5=L: \quad f(C1, C2, C3, C4, C5, C6, N, L) = 0$$

$$\text{Eq. (3.24):} \quad g(C1, C2, C3, C4, C5, C6) = 0$$

$$\text{Eq. (3.25):} \quad h(C1, C2, C3, C4, C5, C6) = R$$

The solution is found by following the Find command in the Mathcad program:

$$\begin{pmatrix} C1 \\ C2 \\ C3 \\ C4 \\ C5 \\ C6 \\ N \end{pmatrix} := \text{Find}(C1, C2, C3, C4, C5, C6, N)$$

The full Mathcad code for the bristle of a rotating cleaning brush described above is presented on the Civil and Mechanical Engineering web site [9].